Focus: HOPE

Manufacturing & Research

1400 Oakman Boulevard, Detroit, MI 48238

FINAL REPORT

MANUFACTURING SYSTEMS DEMONSTRATION: BIMETALLIC FRICTION STIR JOINING OF AA6061 AND HIGH HARDNESS STEEL

May 31, 2013

Primary Author:
Richard Miller
Focus: HOPE
richard.miller@focushope.edu
(313) 494-4716

Submitted to: U.S. Army Tank and Automotive Research and Development Center (TARDEC)
under Contract # W56HZV-05-C-0721, Work Directive WD-FH-0005

Report Documentation Page

Form Approved
OMB No. 0704-0188

1. REPORT DATE	2. REPORT TYPE	3. DATES COVERED
31 MAY 2013	**Final Report**	**18-01-2013 to 15-04-2013**

4. TITLE AND SUBTITLE
MANUFACTURING SYSTEMS DEMONSTRATION: BIMETALLIC FRICTION STIR JOINING OF AA6061 AND HIGH HARDNESS STEEL

5a. CONTRACT NUMBER
W56HZV-05-C-0721

5b. GRANT NUMBER

5c. PROGRAM ELEMENT NUMBER

6. AUTHOR(S)
Richard Miller

5d. PROJECT NUMBER

5e. TASK NUMBER

5f. WORK UNIT NUMBER
WD-FH-000

7. PERFORMING ORGANIZATION NAME(S) AND ADDRESS(ES)
Focus: HOPE,Manufacturing & Research,1400 Oakman Boulevard,Detroit,Mi,48238

8. PERFORMING ORGANIZATION REPORT NUMBER
; #24063

9. SPONSORING/MONITORING AGENCY NAME(S) AND ADDRESS(ES)
U.S. Army TARDEC, 6501 East Eleven Mile Rd, Warren, Mi, 48397-5000

10. SPONSOR/MONITOR'S ACRONYM(S)
TARDEC

11. SPONSOR/MONITOR'S REPORT NUMBER(S)
#24063

12. DISTRIBUTION/AVAILABILITY STATEMENT
Approved for public release; distribution unlimited

13. SUPPLEMENTARY NOTES

14. ABSTRACT
Focus: HOPE (FH) has developed the process parameters to successfully join AA6061 aluminum alloy and High Hardness Armor (HHA) steel using the friction stir process (FSP). Metallographic analysis conducted at the FH metallurgical laboratory, and later at the TARDEC metals lab, has confirmed that the dissimilar metals were metallurgically bonded at the joint surface with a thin (2-5 μm) Al-Fe intermetallic present. Mechanical load testing determined that the bimetallic FSP joint was stronger than similar AA6061-to-AA6061 fusion-welded and FSP joints.

15. SUBJECT TERMS

16. SECURITY CLASSIFICATION OF:			17. LIMITATION OF ABSTRACT	18. NUMBER OF PAGES	19a. NAME OF RESPONSIBLE PERSON
a. REPORT	b. ABSTRACT	c. THIS PAGE			
unclassified	**unclassified**	**unclassified**	**Public Release**	**50**	

LIST OF APPENDICES

LIST OF TABLES

LIST OF FIGURES

A. EXECUTIVE SUMMARY

Focus: HOPE (FH) has developed the process parameters to successfully join AA6061 aluminum alloy and High Hardness Armor (HHA) steel using the friction stir process (FSP). Metallographic analysis conducted at the FH metallurgical laboratory, and later at the TARDEC metals lab, has confirmed that the dissimilar metals were metallurgically bonded at the joint surface with a thin (2-5 µm) Al-Fe intermetallic present. Mechanical load testing determined that the bimetallic FSP joint was stronger than similar AA6061-to-AA6061 fusion-welded and FSP joints.

Initial process parameter trials were conducted to define the operating envelop for this FSP application. FH then evaluated the friction stir process parameters using an orthogonal array methodology. The parameters studied included tool rotation speed, tool traverse rate, tool tilt angle, plunge tool rotation speed, plunge rate, dwell, and joint offset. Other factors that were evaluated include tool design, fixture cooling, and auxiliary induction heating. In total 123 sets of process parameters were evaluated.

Using the process parameter set which exhibited the greatest tensile strength FH produced a series of joint coupons which were then machined into test specimens for mechanical characterization. Metallographic samples were also prepared and analyzed using optical microscopy, scanning electron microscopy (SEM), electron back scatter diffraction (EBSD) and energy dispersive X-ray spectroscopy (EDS).

This report also includes a description of the induction pre-heating system that was designed and demonstrated during this project for the potential use for FSP of high hardness metal alloys.

A summary list of this project's findings and conclusions is in Section G.1 which begins on Page 36 of this report.

B. PROJECT OBJECTIVES

1. Optimize the process parameters to achieve the best possible mechanical and metallurgical properties of a friction stir joint between AA6061[1] and HHA steel[2] with the goal of attaining a tensile stress equivalent to or greater than that of a comparable AA6061-to-AA6061 FSP joint.
2. Perform mechanical testing and metallurgical analysis to characterize the joint material.
3. Design, build and demonstrate an auxiliary work piece pre-heating system to combat FSP tool wear for joining a high hardness material, e.g. armor steel or titanium alloy.
4. Assess the technical feasibility of joining dissimilar materials with the friction stir process.

C. DESCRIPTION OF FRICTION STIR PROCESSES

Friction stir welding (FSW) is a metal fabrication process used to join separate pieces of metal and is a specific application of the friction stir process. However unlike traditional fusion welding processes which use electrical or heat energy to melt the adjoining surfaces of the metal pieces to fuse the material together, FSW is a solid state process where the frictional heat of a rotating machine tool warms the metal/alloy to a temperature that is below its melting/solidus temperature yet softens the metal to a state of plasticity where it can be easily deformed. During the FSW process, the rotating FSW tool stirs the warmed metal of the adjoining surfaces to mix the softened materials thereby welding the pieces together. Figure 1 depicts the features, terminology, and process parameters of the friction stir process. Similar heated stir processes which are fundamentally identical to friction stir processes but use other heating methods include laser, oxyacetylene, induction, and ultrasonic. Heated stir processes are also used as a method to create a metal matrix composite surface layer by introducing metallurgic additives, or to simply refine the grain structure of an alloy.

Figure 2 provides a time-based graphical representation of a typical friction stir process by simultaneously comparing several friction stir process parameters. To begin, the spindle motor rotates the FSP tool at an initial rate which is usually significantly higher than the in-process rotation speed and the machine CNC system moves the spindle to the start position where it is oriented at the proper tilt angles. The rotating tool is slowly lowered (plunged) into the start point of the joint along the plunge axis which is the resultant angle of the back and side tilt of the tool axis. When the FSP tool reaches its final plunge axis weld position, the rotating tool is held at the position for a specified dwell period to fully heat the material. The rotational speed of the FSP tool during the dwell period may remain at the initial speed, lower to a mid-range speed, and/or lower to the final in-process spindle speed. At the end of the dwell, the machine begins to move the rotating FSP tool along the joint axis. Depending on material, design, and

[1] MIL-DTL-32262: Detail Specification, Armor Plate Aluminum Alloy, Unweldable Applique 6061
[2] MIL-DTL-46100E: Armor Plate, Steel, Wrought, High-Hardness

fixture configuration, the process parameters may be varied during the traverse process. Upon completion of the tool traverse, the tool is withdrawn from the material leaving an exit hole.

Because the microscopic structure of a metal is significantly changed after it undergoes a melting and resolidifying transition, the material strength of a fusion weld joint is significantly reduced—as much as 80% for some structural metal alloys. Because it is a solid-state process occurring below an alloy's solidus temperature, a heated stir process avoids the deleterious microstructural transformations that are common with liquid-state fusion welding and virtually eliminates the material porosity inherent with liquid alloy processes. Also because less heat is input to the material during a heated stir process, the volume of material affected by the process heat is substantially lower than that of heat-intensive fusion processes. Another secondary benefit of heated stir joining processes is their capability of joining dissimilar metals which cannot be welded using traditional fusion welding. Because melting temperatures often promote chemical reactions between different material compounds, bimetallic fusion welding i.e. aluminum-steel, aluminum-titanium, titanium-steel is difficult, if not impossible. However because heated stir processes avoid the high temperatures causing these adverse effects, they are more applicable to joining dissimilar alloys

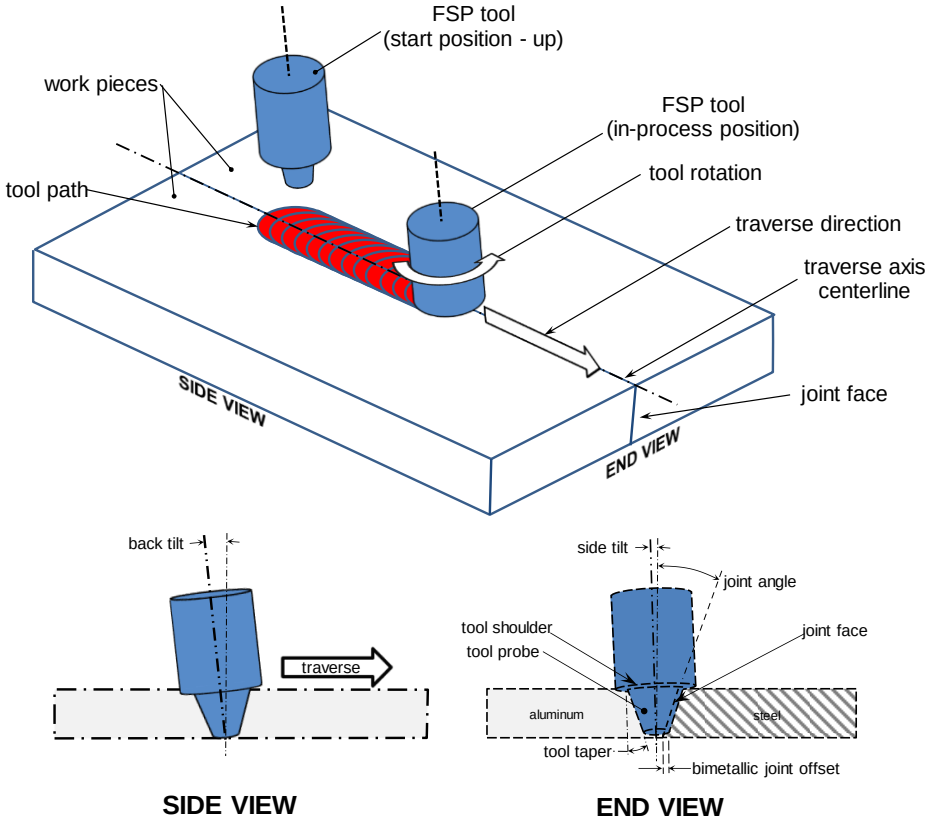

Figure 1 – FSP Terminology

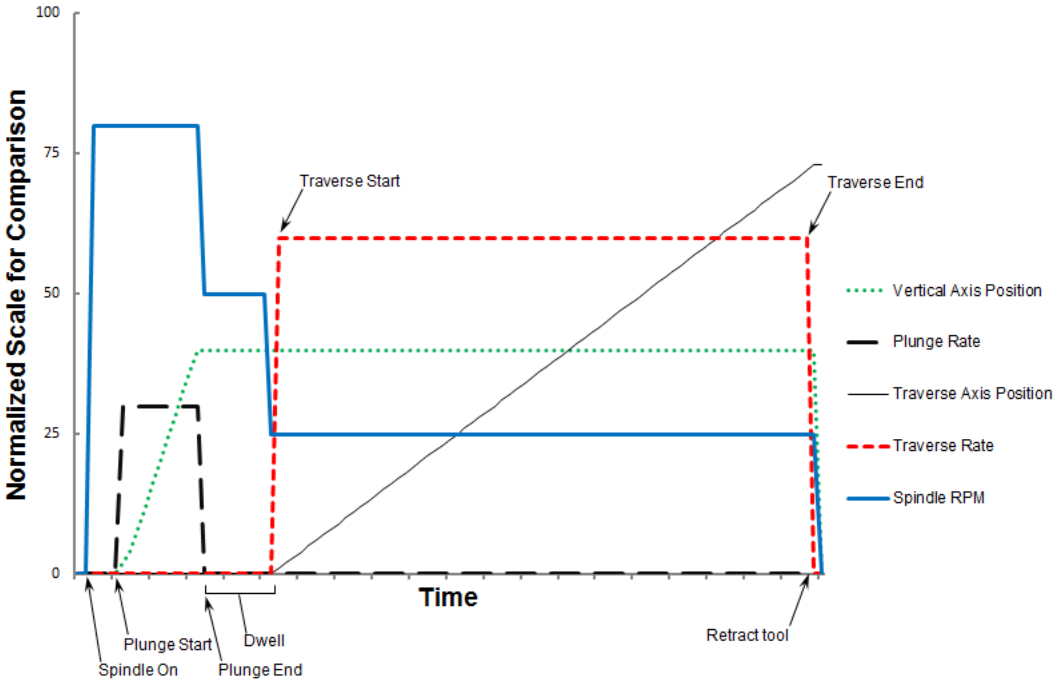

Figure 2 – FSP Process Graph

1. Machine and Fixture Descriptions

a) Friction Stir Machine – All joining was done on the Transformation Technologies Inc. (now MTI) GG1 Series friction stir machine located at the FH facility (Figure 3). This machine features a 6-axes CNC system, separate FSP tool and fixture cooling circuits, force/torque monitoring, and control sensors and software. Table 1 lists the motion and load specifications for the machine.

Figure 3 – TTI Series GG1 Friction Stir Machine

Table 1 – TTI GG1 Specifications (maximums)

		Travel	Travel Rate	Load
X-Axis	Horizontal	1525 mm	1800 mm/min	67 kN
Y-Axis	Horizontal	2550 mm	1800 mm/min	67 kN
Z-Axis	Vertical	1270 mm	1800 mm/min	67 kN
A-Axis	Primary rotation	±182.5°	1200 °/min	4500 Nm
B-Axis	Secondary rotation	+130°/-50°	1200 °/min	4500 Nm
C-Axis	Turntable	- - -	1350 °/min	8500 Nm
Spindle	15 kW drive	- - -	100-3000 rpm	186 Nm

b) Weld Coupon Fixture – All joint material coupons were fabricated using the fixture that was originally custom-made for the WD-FH-0004 work directive (Figure 4). The fixture has two design configurations for different final coupon sizes: ½" thick x 2" wide x 8" long or 1" thick x 4" wide x 8" long. All material used for this bimetallic project was ½" thick x 1" wide bar stock. The lower platen of the fixture is ported for liquid cooling with each work piece position having separate distribution manifolds so that heat can be extracted for either or both of the work pieces. During the process envelop trials of this project, the aluminum side of the joined coupons exhibited

excessive flaws which we attributed to the aluminum reaching a liquid state. By re-routing the fixture coolant system flow to entirely pass through only the aluminum side of the fixture, the heat extraction from the aluminum was improved and the liquid state flaws were reduced or eliminated, depending on the tool rotation speed. This was further improved by replacing the aluminum-side clamp bar with a ported bar that was installed in-series with the flow of the fixture coolant.

We fabricated a short series of coupons using the best parameter set to determine if the use of the cooled clamp bar (without induction pre-heating) on the aluminum side affected joint strength. The results of this experiment results indicate that the removal of the cooled clamp bar degraded joint tensile strength approximately 15-20 MPa.

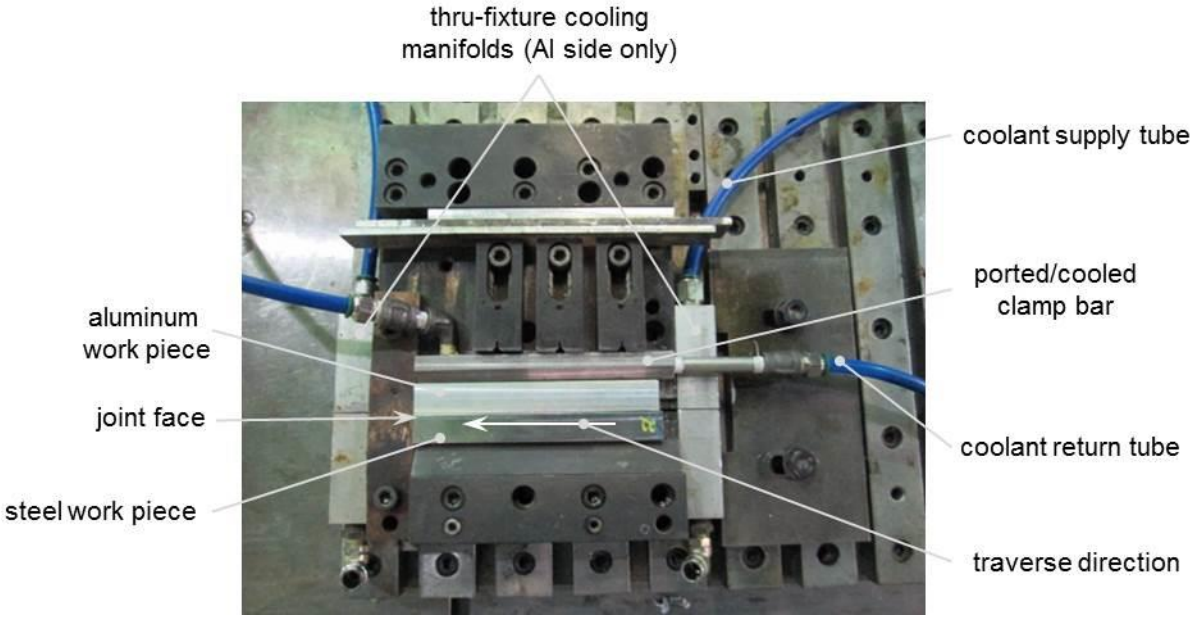

Figure 4 – FSP Work Piece Fixture

2. Friction Stir Tools

a) Design – Based on the FSP tool design and development that had been done during the WD-FH-0004 work directive, all coupons were fabricated using a tool as shown in Figure 5 which has a 1.0-inch diameter shoulder, 0.480-inch probe length, and 12.0° probe taper. The tapered probe design allows worn tools to be repeatedly dressed via machine grinding to extend the tools' overall life. Several tools experienced in-process failures by fracturing at the shank or probe base, or exhibiting excessive probe wear. These tool issues are further discussed in D.4.a.

b) Material Selection – The FSP tools were made from several tungsten-based materials: W-25%Re, W-25%Re-2%HfC, and W-La. The W-25%Re alloy tools exhibited the best durability. The W-25% Re-2%HfC alloy tools had good wear-resistance but failed by fracturing, and the W-La tools exhibited unacceptable wear. These tool issues are further discussed in D.4.a.

Figure 5 – New FSP Tool with Tapered Probe

3. Process Parameter Optimization Experiments

a) ***Description -*** Based on a FSP process parameter operating envelop that was established during the WD-FH-0004 project, a parameter set based on best tensile strength was developed. For simplicity and expedient testing, the tensile tests conducted during this parameter development stage used 3/16-inch thick x ½-inch wide x 2-inch long transverse test specimens that had been cut perpendicular to the joint axes with the laboratory water-cooled abrasive saw. The specimens were placed into the Instron universal load tester with the steel side held by one jaw and the aluminum side held by the opposing jaw. Several separate specimens from each coupon were tested to assess the strength level of the particular process parameter set. While not a standardized test, this method provided us with quick measurements of the joint strength.

The FSP process parameters, and their ranges, that were evaluated during this stage are listed in Table 2. All experiments were run with machine positional control with the vertical (Z) and transverse (X) axes zeroed for each run which compensated for varying work piece dimensions and tool probe length. For many coupons, two similar sets of parameters were used for a single coupon, for example the first half of the joint was fabricated with a traverse speed of 40 mm/min and without stopping the second half was produced with a slightly slower 35 mm/min. For these cases the coupons were identified with a sequential number—as was all coupons—and letter designations “A” and “B” for the first and second parameter sets respectively.

Table 2 – FSP Process Parameters and Ranges

	Min.	Max.	Best
Tool rotation speed (rpm)	200	400	250
Traverse speed (mm/min)	10	50	40
Joint offset (mm)	0	1.5	1
Back tilt (degrees)	2.0	3.0	3.0
Side tilt (degrees)	0	0.8	0.21
Pre-heating parameters	see Section F		- - -

b) ***Experiment Results*** – The parameter set shown in the last column of Table 2 resulted in a best coupon mean tensile strength of 205 MPa for Coupon #40. Two other coupons, #56 and #66, that were fabricated using this best parameter set, but on different dates, exhibited similar strength levels, 194 MPa and 183 MPa respectively, with a maximum single test of 223 MPa from Coupon #56.
Table 3 summarizes the parameter sets and tensile test results for the FSP process parameter optimization experiments. Not included in this table are the coupons that were fabricated using an auxiliary heating system 1-19 and 41-48 (See Section F), exhibited visual discontinuities, or experienced a broken tool.
Two general trends are apparent when the results are viewed graphically. First as seen in Figure 6, tensile strength increases as traverse speed is increased for the speed range evaluated. 50 mm/min was chosen as the upper limit for traverse speed to avoid machine axis overloading based on machine load data observed during previous trials. Second, at tool rotation speeds above 250 rpm tensile strength decreases as tool rotation speed is increased. During these and previous parameter experiments, visual discontinuities and/or excessive aluminum melting were common with tool speeds greater than 350 rpm.

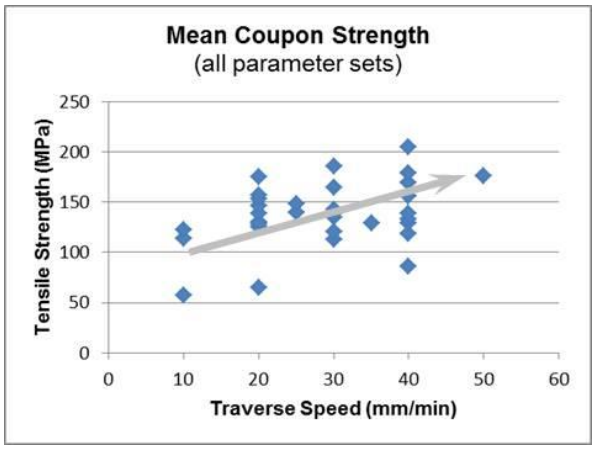

Figure 6 – Data Trend for Tensile Strength vs. Traverse Speed

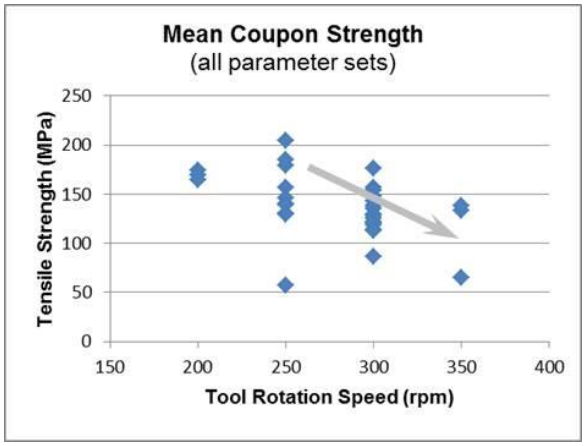

Figure 7 – Data Trend for Tensile Strength vs. Tool Rotation Speed

Table 3 – FSP Process Parameter Optimization Tensile Test Results

Coupon[1]	Tool Rotation Speed (rpm)	Traverse Speed (mm/min)	Joint Offset (mm)	Back Tilt (°)	Side Tilt (°)	Specimen Quantity	Mean Tensile Strength (MPa)
20	250	25	1.0	3.0	0.00	3	139.9
21A	250	10	1.0	3.0	0.00	3	57.3
21B	250	20	1.0	3.0	0.00	2	65.3
22A	250	30	1.0	3.0	0.00	3	138.8
22B	250	35	1.0	3.0	0.00	1	128.9
23	250	20	1.0	3.0	0.00	3	146.1
24A	350	40	1.0	3.0	0.00	5	138.4
25A	250	20	0.5	3.0	0.00	4	156.8
25B	350	40	0.5	3.0	0.00	4	133.2
26B	400	30	1.5	3.0	0.00	5	133.9
28A	250	40	1.5	3.0	0.00	3	178.7
28B	300	50	1.5	3.0	0.00	3	176.0
30	350	30	2.0	3.0	0.00	2	135.8
32	300	25	1.0	3.0	0.00	6	112.0
34A	200	20	1.0	2.0	0.00	5	174.7
34B	250	30	1.0	2.0	0.00	4	185.4
35	300	40	1.0	2.0	0.21	5	156.3
36	250	20	1.0	2.5	0.21	6	130.4
37A	300	30	1.0	2.5	0.00	6	142.9
37B	200	40	1.0	2.5	0.00	6	169.4
39A	300	20	1.0	3.0	0.21	6	153.4
39B	200	30	1.0	3.0	0.21	5	164.7
40	250	40	1.0	3.0	0.21	5	204.5 BEST
53 [2]	250	40	1.0	3.0	0.21	5	182.3
54A	250	40	1.0	3.0	0.20	3	140.9
54B	250	25	1.0	3.0	0.21	5	132.4
55	250	35	1.0	2.5	0.17	5	152.3
56	250	40	1.0	3.0	0.40	8	194.0
57	250	40	0.5	3.0	0.42	5	180.6
58	250	40	0.5	3.0	0.70	5	150.2
59	250	40	0.5	3.0	0.70	2	135.1
60 [3]	250	40	1.0	3.0	0.63	2	161.9
61	250	40	1.0	3.0	0.32	5	165.9
62	250	40	1.0	3.0	0.21	5	159.8
63	250	40	1.0	3.0	0.00	4	148.4
64	250	40	1.0	2.5	0.32	4	136.6
65	250	40	1.0	2.0	0.32	2	154.8
66	250	40	1.0	3.0	0.65	4	182.7
76 [4]	250	40	1.0	3.0	0.78	3	140.4
77	250	40	0.5	3.0	0.67	4	129.9
78	250	40	1.0	3.0	0.67	5	146.5

[1] *Coupons with visual defects were not tested.*
[2] *Without aluminum side cooled clamp bar.*
[3] *For Runs 60 and later, a positional offset to correct the A and B rotational axes angles was used.*
[4] *Cooling system corrections (tube routing, tank filled)*

During this stage of process parameter development, two joint failure modes were observed. The first, shown in Figures 8a and 9a, was occurred with the better performing tensile tests. This ductile fracture occurred solely in the aluminum alloy away from the joint face in the thermo-mechanically affected zone (TMAZ) of the FSP joint (as determined in subsequent micro-hardness analysis—See Section E.1.c). The second failure mode, shown in Figure 8b and 9b, exhibited brittle fracture in the aluminum alloy adjacent to the joint face for approximately one-half of the joint face. The remaining portion of the joint face did not indicate that bimetallic bonding occurred and that the steel and aluminum materials simply separated in this region.

Figure 8 – Tensile Failure of Bimetallic Joint (side view)

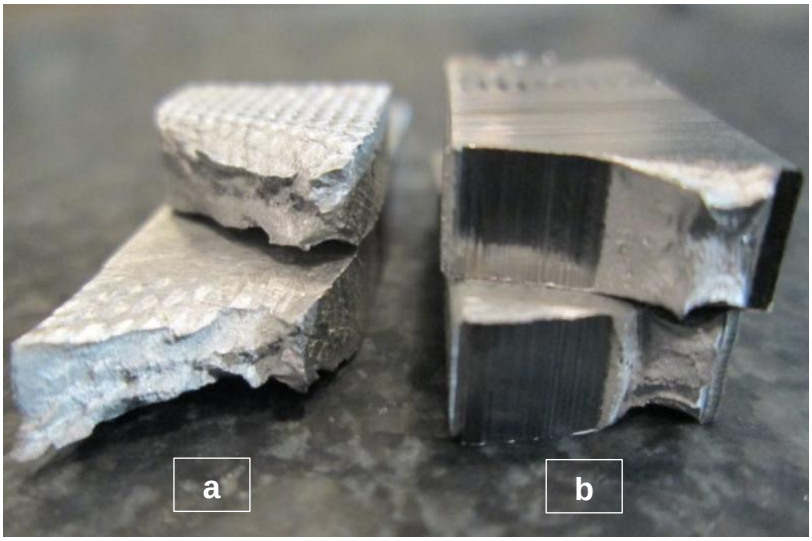

Figure 9 – Tensile Failure of Bimetallic Joint (end view)

4. Issues and Obstacles

a) ***Friction Stir Tool Failures*** – The first of two issues that affected this project was the failure of several FSP tools which temporarily depleted our tool inventory and delayed the FSP parameter development experiment stage. Three distinct failure modes were apparent and are shown in the photos of Figure 10.

Figure 10 – FSP Tool Failures

a) Broken probe (W-25%Re-4%HfC)
b) Typical probe wear (W-25%Re)
c) Excessive probe erosion (W-La)
d) Broken shank #1, side view (W-La)
e) Broken shank #1, axis view (W-La)
f) Broken shank #2, side view (W-25%Re-4%HfC)
g) Broken shank #2, axis view (W-25%Re-4%HfC)

Figure 10a shows a FSP tool without its probe which had separated from the tool at the shoulder. The probe section remained lodged in the incomplete joint coupon. This failure occurred on three tools all of which were machined from separate rod stock of 1.00-in. diameter tungsten-rhenium (25%) having either 2% or 4% hafnium carbide content. For two of these tools, the failure occurred at the beginning of the traverse motion on the particular tool's first use. In all tools made of alloy having hafnium carbide, we've commonly seen small voids (0.0-1.0 mm dia.) on the surface of machined tools and for one particular tool failure identified that its failure occurred at the location of a void located at the base of the probe. Despite the supplier's (Rhenium Alloys Inc., Elryia, OH) contrary opinion we believe that these material discontinuities are the cause of this type of failure. A new tool was fabricated from non-HfC W-25%Re alloy and was used for the remainder of the project without incident.

Figure 10b shows a used tool which exhibits the typical wear and use characteristics. Residual aluminum material from the work piece covers most of the shoulder and probe surfaces and the actual tool material (dark color) can be seen on the lower section of the probe (small diameter end of taper). Also visible at the tip of the probe is a small disk of aluminum material. Closer examination shows that the tungsten alloy material of the tool typically shows its wear in the form of a slight radius forming at the probe tip and small shallow wear grooves around the perimeter surface of the probe.

Figure 10c shows the second type of tool failure seen during the project; excessive material erosion and wear. The remnants of this probe are about half the size of its original shape with this tool having completed only one 6-in. long bimetallic weld. Figure 10d also show this probe and shoulder wear after only a single plunge stage of a FSP coupon fabrication. Both of these tools were made from lanthanated tungsten (W-La) alloy which indicates that this particular alloy is unable to withstand the rigors of FSP.

Figures 10d and 10f are the side views of two tools that fractured at the tool-holding shank section. Figures 10e and 10g are the central end views of the fracture surfaces. Both of these failures occurred after the plunge stage when the traverse motion began. The cause of these failures was simply a design flaw. The views on the right side of Figures 10e and 10g show that the fracture occurred at the inside radius of the tool's internal cooling port. Figures 10d and 10f also show that the fractures occurred near the edge of one of the four machined set screw flats on the exterior of each tool. Post-failure design analysis determined that this area of the tool had the smallest cross-sectional area because of the confluence of the end of the internal cooling port and four external tool-holding flats. The tool design was subsequently revised to reduce the depth of the cooling port and to delete three of the tool flats.

b) ***Changes in Spindle Loading*** – Following the final series of parameter experiments which studied back and side tilt combinations, Coupon #66 was fabricated using the best parameter set and tensile tested as a final confirmation of the strength repeatability of the best parameter set which was established at Coupon 40 and previously confirmed by Coupon 56. However the average tensile strength for Coupon 66 fell nearly 11% below the best strength of Coupon 40 (183 MPa and 205 MPa respectively). While this decrease in tensile strength was noted, because of the impending project deadline, the best parameter set was used to fabricate a series of coupons from which the final mechanical characterization specimens would be machined.

After several of these final coupons were fabricated (67-75), the FSP spindle load data were reviewed for process monitoring, as it was done throughout the parameter development stage. The coupon-to-coupon traverse force data exhibited a definite trend of increasing loading particularly through the second half of the joint traverse.

Figure 11 includes a comparison of the process loads of cross-feed force (X-axis), forging force (tool centerline axis W), spindle torque, and traverse force (Y-axis) for Coupons 68 through 75 [3] which were all fabricated using identical FSP process parameters. (Slightly different plunge and dwell parameters resulted in start, end, and overall time differences between the data plots.) The cross-feed force and spindle torque were relatively equal for these coupons but the forging and traverse force plots exhibited significant differences. While the graphs exhibited similar shapes for 68-75 with a slight upward slope through the traverse section of the weld, the shape of the confirmation baseline Coupon #66 was generally downward sloping. Furthermore the forging force during the traverse section of 67-75 differed by approximately 30% between the high and low graphs. The traverse force graphs also showed relatively different force levels. The traverse force graphs of Coupons 68-70 are grouped together and follow the basic shape of the confirmation baseline Coupon #66 for the first half of the joint however 68, 69, and 70 all begin increasing with slopes two to three times that of Coupon 66. The traverse forces exhibited by Coupons 72-75 are roughly 2.5 times that of the confirmation baseline coupon and exhibit notable fluctuations throughout the process. The traverse forces at the end of the joint for all of these coupons increased significantly during the second half of the process by reaching levels two to three times that of the traverse forces at the beginning of the traverse section.

The load data of the coupons fabricated using the best parameter set (40, 56, and 66) were also compared. As shown in Figure 12, the overall graph shapes and load levels for Coupons 40, 56, and 66 are notably different in several areas. The cross-feed force of Coupon 66 has a positive slope compared to a slight negative for 40 and 56. While the levels of forging force are similar for 40 and 66, Coupon 56 experienced significantly higher force. Also the traverse force of Coupon 66 is two to three times that of the other two coupons.

Since these data comparisons seemed to indicate that a process change(s) had occurred, we conducted an investigation to determine if any external factors, e.g. machine, fixture, or materials, had caused the apparent change. The following aspects were evaluated:

Spindle angles, actual vs. screen/program value
Machining variations between coupon bars
Relative side tilt angle of joint face and probe surface
Fixture position with respect to machine axes
Traverse axis, X vs. Y
Fixture and tool cooling system

These subsequent troubleshooting experiments exhibited spindle loading differences similar to those observed for Coupons 67-75. Furthermore several of these coupons

[3] The data files for Coupons 67 and 71 were inadvertently overwritten.

were fabricated using the best parameter set yet their average coupon tensile strength was 10-20% lower than the strongest coupons of this project (40 and 56). None of the above factors were found to be adversely affecting tensile strength.

Comparison data and process descriptions were provided to the manufacturer of the friction stir machine (MTI, Inc.) for their review who, having found no clear cause of the observed load irregularities, recommend an on-site diagnostic service review.

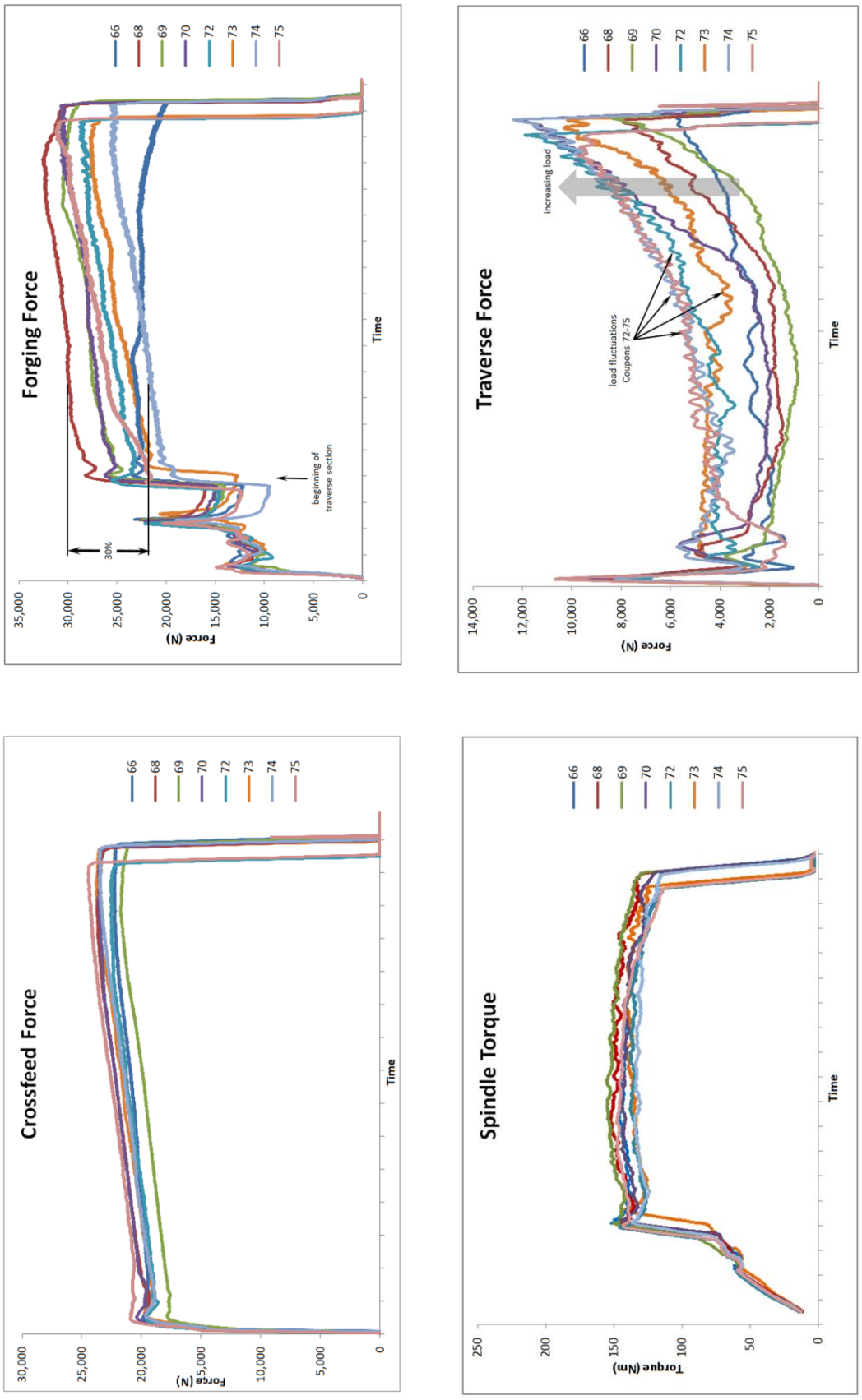

Figure 11 – Spindle Loading (Coupons 66-75)

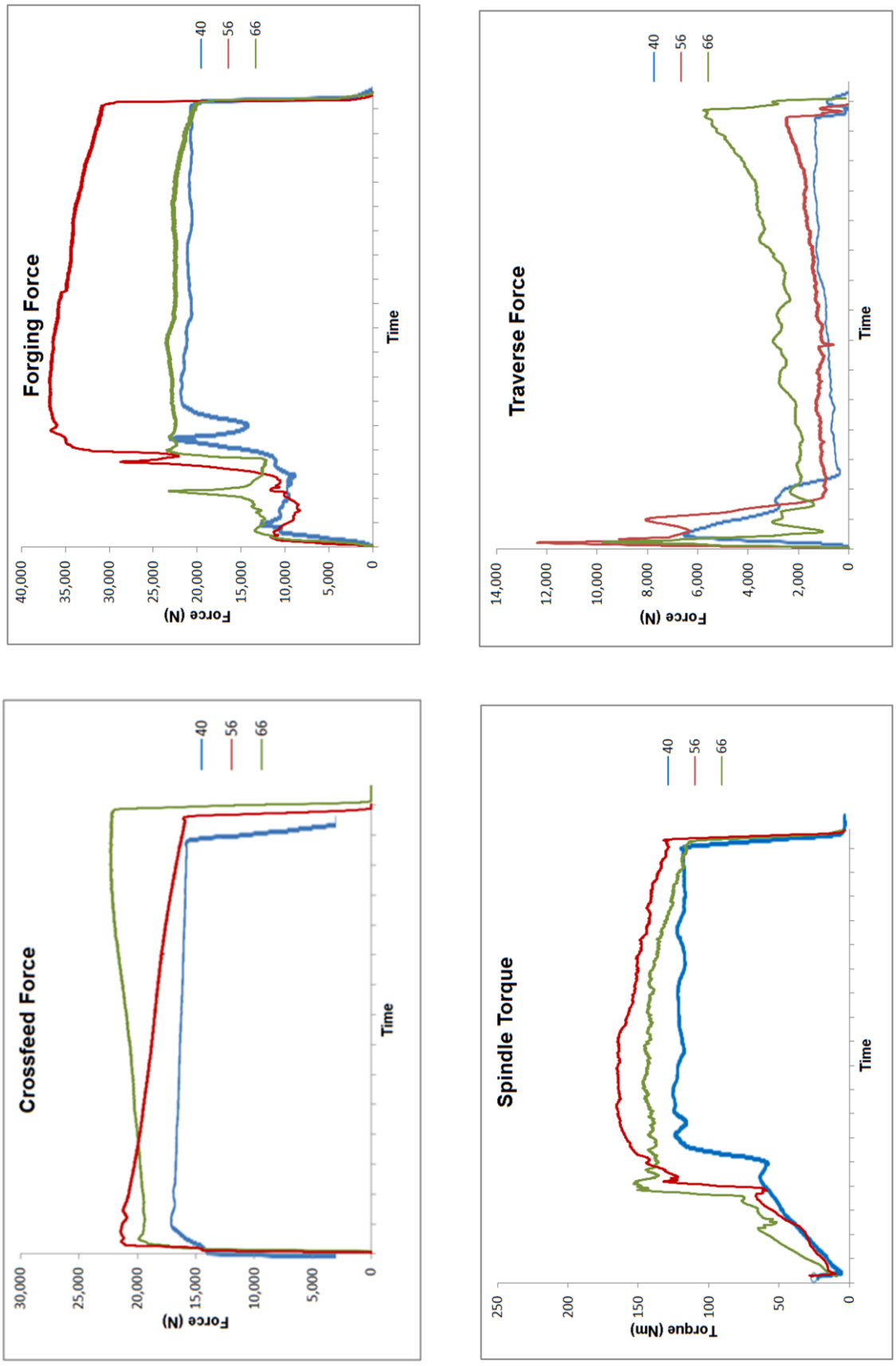

Figure 12 – Spindle Loading (Coupons 40, 56, & 66)

E. FINAL RESULTS

1. Metallurgical Analysis

a) ***Base Material AA6061-T6511*** - Aluminum 6061 is a precipitation hardening aluminum alloy, containing magnesium and silicon as its major alloying elements. The chemical composition of AA6061 plate used in the present study is listed in Table 4. During precipitation heat treatment, silicon combines with magnesium to form Mg_2Si precipitate and contributes to the age-hardening process. AA6061 may be formed in the T4 temper (solution heat-treated) and T6 temper (solution heat-treated followed by precipitation heat-treated). AA6061 has good formability, weldability, machinability, and corrosion resistance, with medium strength.

Table 4 – Chemical Composition of AA6061-T6511 Plate

Element	Al	Si	Fe	Cu	Mn	Mg	Cr	Zn	Ti	Other Each	Others Total
Wt. %	Bal.	0.40-0.80	0.7	0.15-0.40	0.15	0.8-1.2	0.04-0.35	0.25	0.15	0.05 max	0.15 max

Figure 13 shows the micrograph of the as-received AA6061-T6511 plate. The average grain size of the as-received plate was found to be about 200 µm. Note that the microstructures of all samples examined in this project were investigated by a scanning electron microscope (Zeiss EVO MA 10) equipped with an energy-dispersive spectroscopy system (Apollo X, EDAX) and an electron backscatter diffraction (EBSD) system (Hikari camera, EDAX-TSL).

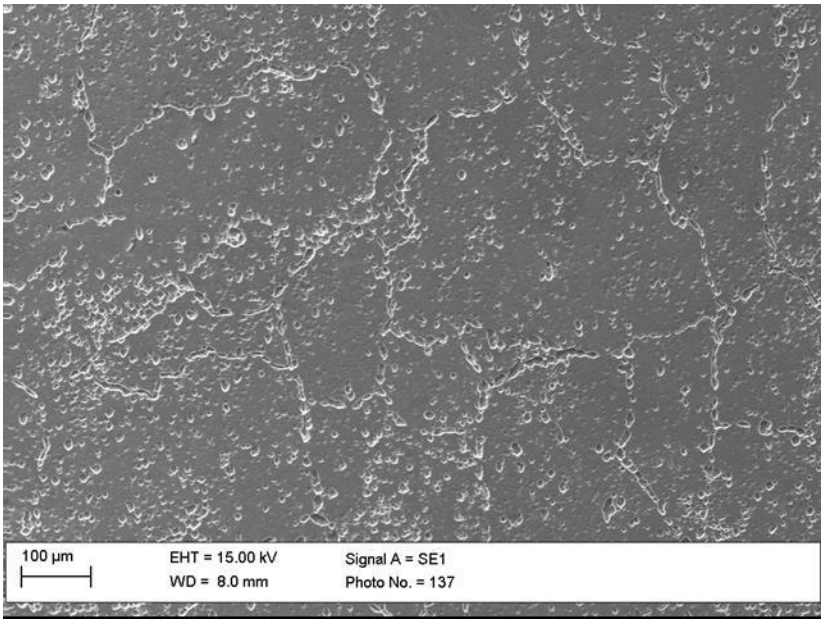

Figure 13 – SEM Micrograph of the As-Received AA6061-T6511

b) ***Base Material MIL-DTL-46100E Steel*** – This alloy is quenched and tempered high-hardness armor (HHA) wrought steel plate for lightweight armor applications for recommended thickness up to 2-inches. HHA steel plates have been used to build armored combat vehicles and vessels due to good ballistic behavior accompanied by weight reduction in the armored structure as a consequence of the plate's high mechanical strength. The chemical composition of MIL-STD-46100E HHA used in the present study is listed in Table 5. The as-received steel plate was quenched and tempered (water quench from 1660 ºF and air tempering at 425 ºF for 71 min).

Table 5 – Chemical Composition of MIL-STD-6100E Steel Plate

Element	Fe	C	Mn	P	S	Si	Cu	Ni	V	Al	Cr	Mo	Ti
Wt. %	Bal.	0.28	0.87	0.011	0.003	0.45	0.05	0.4	0.01	0.041	0.5	0.21	0.045

Figure 14 shows the SEM micrograph of the as-received MIL-A-46100 steel plate which exhibits typical martensitic microstructure that was developed due to the water quenching from 1660 ºF. Note that although the steel plate was quenched and tempered, hardly any cementite or carbide particles are seen in the SEM micrograph. Due to the low tempering temperature (425 ºF), it is expected that the martensitic structure was mainly stress-relieved but not transformed to the tempered martensite structure. Also note that the micro-hardness of the as-received steel plate was found to be about 550 HV. This very high level is the result of martensitic microstructure developed during water quenching.

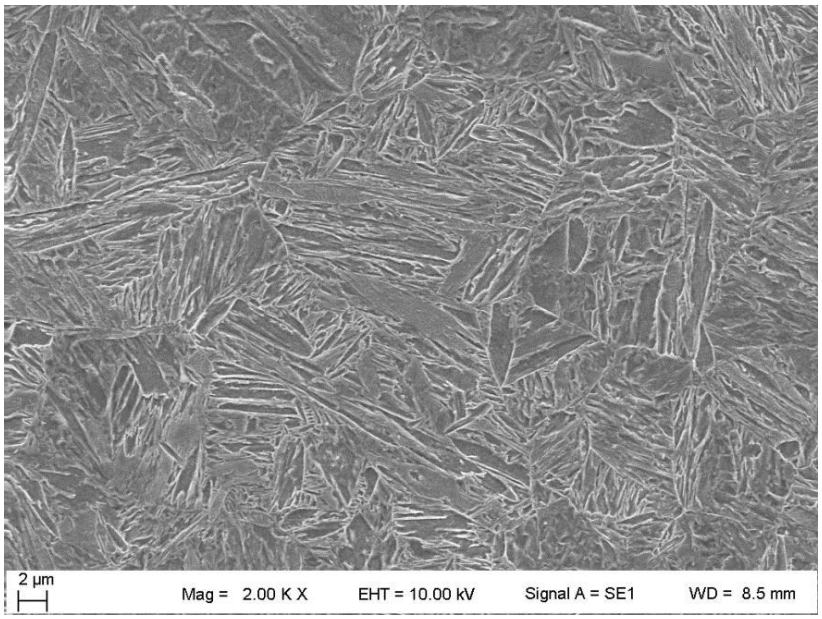

Figure 14 – SEM Micrograph of the As-Received MIL-STD-46100E Steel Plate

c) ***Micro-Hardness Measurement*** - To understand the microstructure and mechanical property variations across the weld, a comprehensive hardness measurement was conducted on the transverse cross-section of the weld as shown in Figure 15a. The micro-hardness measurement was conducted using a LECO MAH43 automatic micro-hardness tester using a 500 gm load on steel and 100 gm load on aluminum for a dwell time of 10 s. To better understand the mechanical response of the weld, micro-hardness measurements were conducted at 1863 points (81 × 23 grid) on a 40 mm × 11 mm transverse cross-section of the bimetallic joint. The distance between two indentations was 0.5 mm. Figure 15b shows the hardness distribution map of the transverse section of the weld.

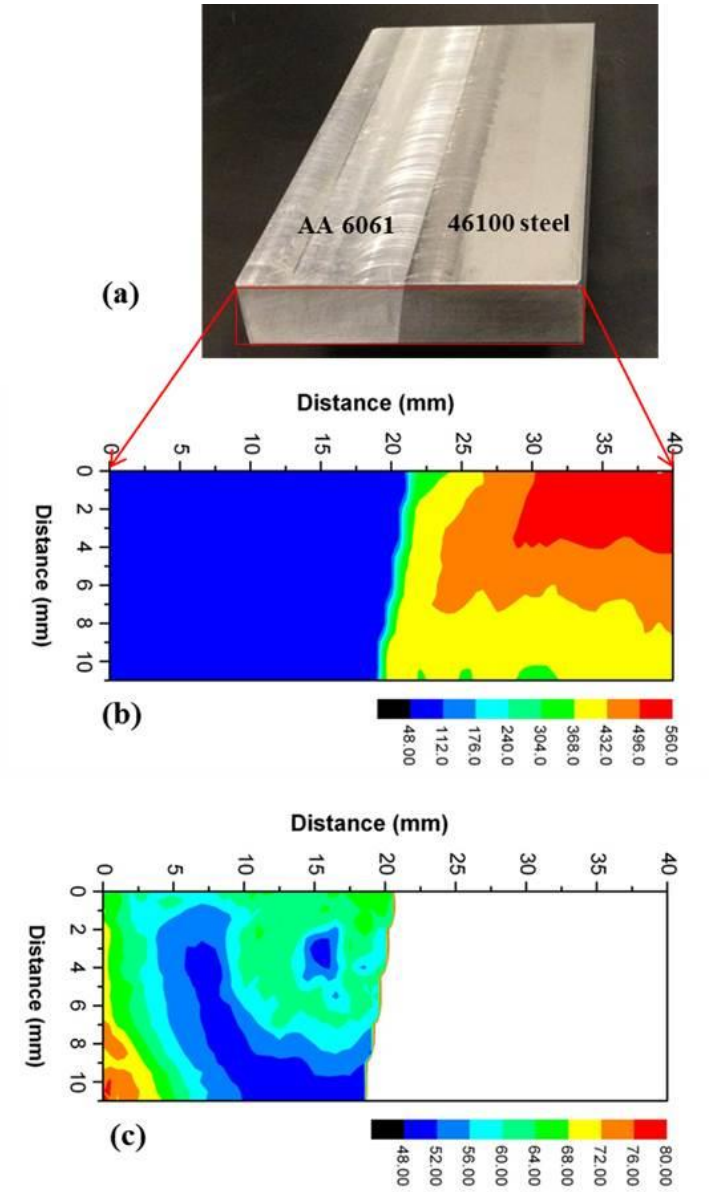

Figure 15 – Micro-Hardness Distribution of Transverse Cross-Section

It is seen from the hardness plot (Figure 15b) that the hardness of the steel plate after welding varies from 304 to 560 HV. Note that a gradual hardness increase was observed from bottom to top and from the bimetallic joint interface to the right edge of the steel plate. However, in the aluminum side only one color (blue) can be seen in the overall plot. Since the hardness of the Al is much lower than the steel, a second hardness distribution map (Figure 15c) was constructed to reveal the minor hardness variation within the aluminum section. It should be noted that the hardness profile of the aluminum side of this bimetallic joint is typical of the profiles exhibited by all-aluminum friction stir joints with heat-treatable Al alloys. Figure 15c shows that the hardness of the heat-affected zone (HAZ) was around 48-56 HV, whereas the hardness of the nugget was found to be about 56-68 HV except a small weak area of hardness around 48-56 HV. Note that the hardness of the as-received AA6061-T6511 plate was 110 HV. The substantial hardness decrease in the HAZ and weld nugget is related to the dissolution of Mg_2Si precipitates in the Al matrix during welding. As-received AA6061-T6511 was fully hardened by Mg_2Si precipitates, however due to the heat generated during the friction stir process, Mg_2Si precipitates partially or completely dissolved in the aluminum matrix depending on the local temperature at different joint locations. It is expected that the temperature of the nugget material was higher than that of the HAZ. However the relatively higher hardness of the nugget compared to the HAZ is the result of grain refinement in the nugget zone by dynamic recrystallization of the severely-deformed aluminum above the recrystallization temperature.

d) ***Microstructural Characterization*** - Figure 16 shows the microstructure of steel at different cross-section joint positions that correspond to different hardness levels. From the hardness map it is seen that the hardness of the steel is lowest at the bottom of the steel side near the bimetallic interface. Figure 16a exhibits the tempered martensitic microstructure that is typical of the lower hardness regions (yellow) of the micro-hardness profile. The middle portion of the steel side (orange) also shows tempered martensitic structure with the hardness of 432-496 HV. On the other hand, the top-right corner of the steel side shows martensitic microstructure and the highest hardness (496-560 HV) which is similar to the hardness of the as-received steel plate. From the micro-hardness profile and microstructural morphology, we conclude that the lower portion of the steel substrate near the bimetallic joint interface slowly cooled after the FSP tool had traversed through this area. As a result, well-tempered martensitic microstructure developed. On the other hand, the top-right corner of the sample was only marginally-affected by the frictional heat of the friction stir process because of its greater distance from the joint interface. As a result, the tempering effect was gradually reduced as the distance from the joint increased and consequently the material hardness gradually increased to a level near that of the as-received steel plate.

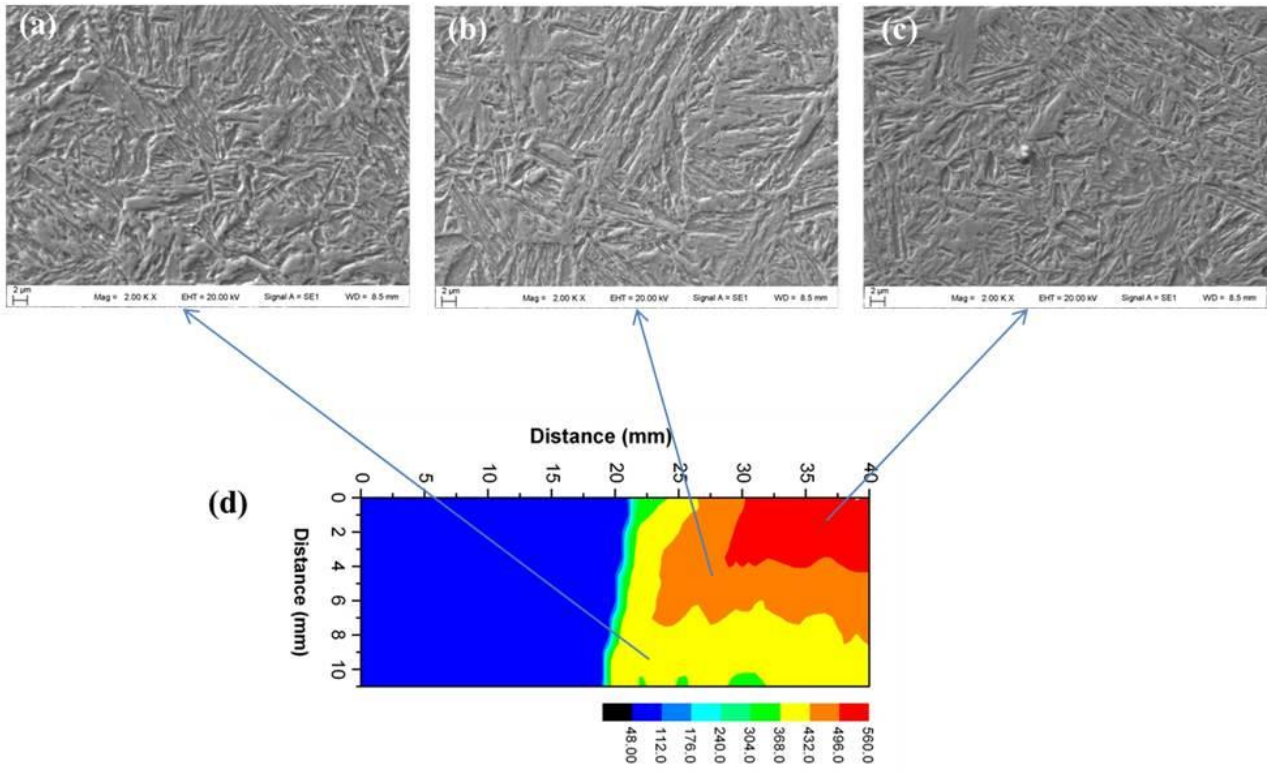

Figure 16 – Microstructure of Steel at Different Joint Positions

e) ***EBSD Investigation*** - The microstructural morphology of the aluminum material at different positions of the joint was investigated using EBSD as shown in Figure 17. The EBSD investigation revealed that the grain size of the nugget zone was reduced to about 5-10 µm. Note that the grain size of the as-received AA6061-T6511 plate was 100-500 µm. During the friction stir process, the material in the nugget zone underwent severe plastic deformation at high temperature. Consequently, this stir zone material dynamically recrystallized to smaller grains. The microstructure of the HAZ shows the existence of sub-grain within the large grain. The EBSD color contrast of these grains suggests that the orientation of the sub-grains remain close to the parent grains. This sub-grain was probably developed by poligonization during thermal excursion because of the heat generated by the friction stir process.

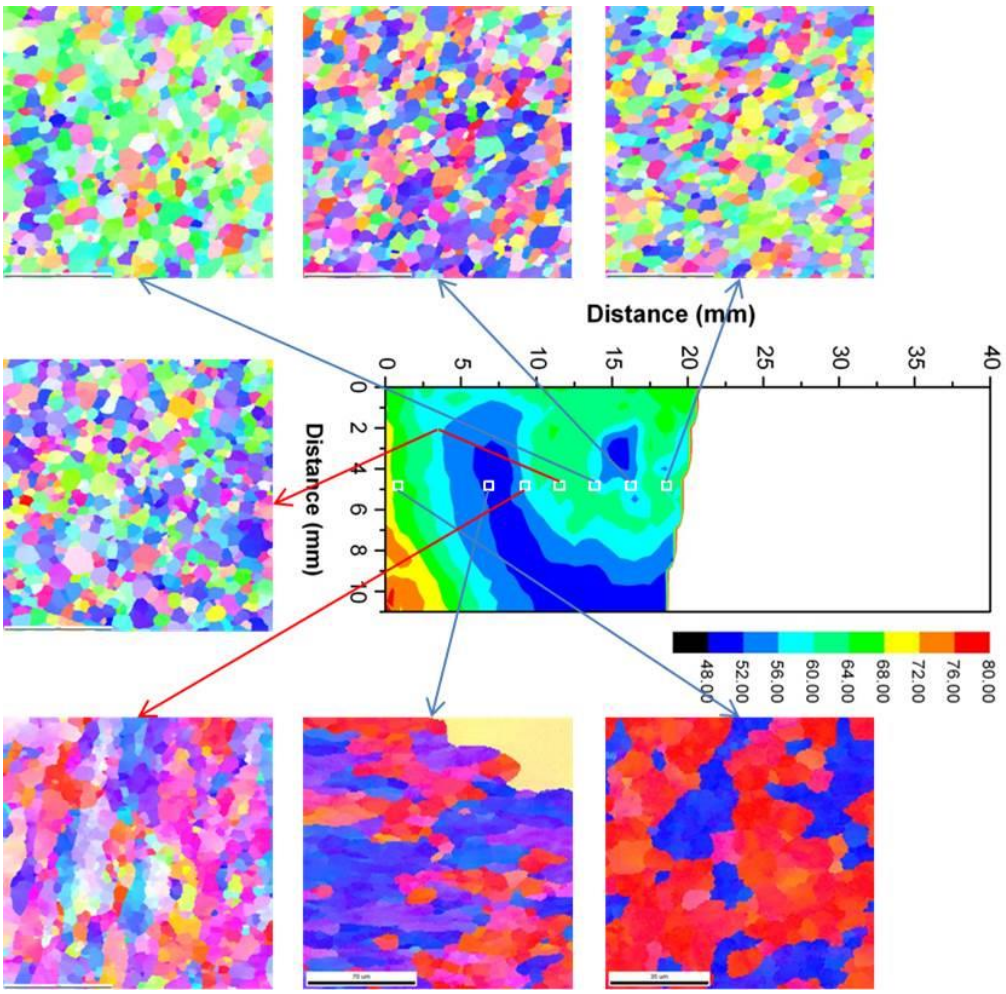

Figure 17 – Microstructural Morphology of Aluminum Grains at Different Joint Positions

f) ***EDS Investigation*** - Energy dispersive spectroscopy (EDS) investigation was used to evaluate the elemental distribution within the bimetallic joint material. Figure 18 depicts the elemental map at the joint interface and reveals that a 1-2 µm thick diffuse layer of aluminum and iron was developed at the joint interface. Note that the diffuse layer was relatively thicker at the upper part of the weld compared to the lower part. This is due to the relatively larger amount of heat that is generated by the FSP tool at the substrate/tool shoulder interface along the top surface of the joint.

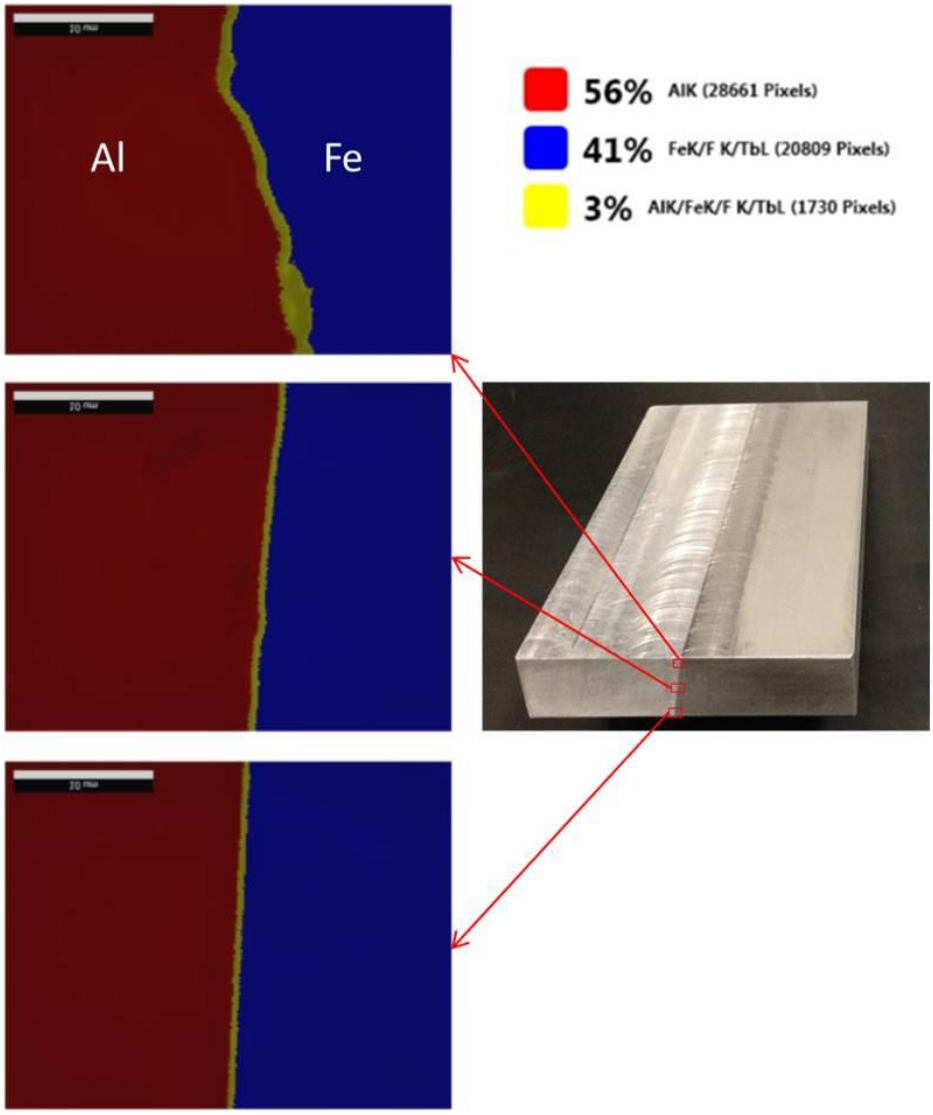

Figure 18 – Elemental Map Across the Bimetallic Joint Interface

2. Mechanical Load Tests

a) ***Specimen Preparation*** – The bimetallic joint specimens were extracted from a series of joint coupons that were fabricated using the best FSP parameters. After the friction stir process, the top and bottom surfaces of the coupon were milled to remove weld flash and to square the material. Both ends of each coupon where the plunge position and exit hole are located were removed using a water-cooled laboratory abrasive saw. The final 0.48-in. thick x 2.0-in. wide x 5-in. long joint coupons were then waterjet cut into bimetallic joint samples. Three sample configurations of size and joint orientation were then the starting point for final specimen machining. See Appendix B for design drawings of the coupon extraction and final machined specimens. Figure 19 depicts the test specimens and their respective orientation with the bimetallic joint face/axis.

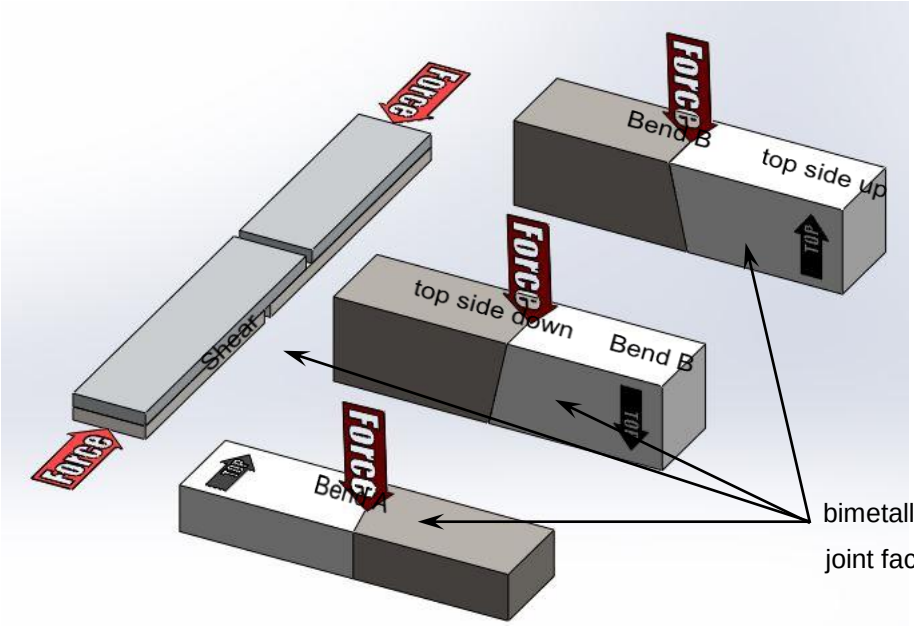

Figure 19 – Bimetallic FSP Joint Specimens: Bend A, Bend B, and Shear

As discussed in Section 4.B, machine repeatability issues limited the quantity of final coupons that were available for preparation of final test specimens. Because tensile test data existed for the best parameter set, these coupons were used to fabricate shear and bend test samples only.

Since AA6061 is a heat-treatable alloy, we also conducted a small study to determine how heat treatment affected the bimetallic joint strength. The T6511 heat treatment specification requires both solution and aging processes (See Table 6). Because the solidus point temperature of the steel alloy (1400 °C) was significantly greater than that of the aluminum alloy (582 °C) any heat treatment temperature that would affect the steel would significantly degrade the aluminum. Therefore only aluminum heat treatment was conducted for this study.

Table 6 – AA6061-T6511 Heat Treatment Specifications

Solution		Percipitation (Aging)	
Temperature	Time	Temperature	Time
530°C	1 hour	175°C	8 hours

Three configurations of bend test specimens were analyzed: full heat treatment, precipitation only, and as-welded. Table 7 tabulates the bend test results of the heat treatment comparison study which indicates that the aging-only process produced a slightly higher bimetallic joint strength than if the material had not been heat treated. For both the Bend A and Bend B test specimens, the full T6511 heat treatment process drastically lowered the bimetallic joint strength compared to the aging only and as-welded specimens. This is probably because the relatively higher solution heat treating temperatures promoted additional formation of brittle Al-Fe intermetallic at the joint interface which resulted in the brittle fractures that were observed for those bend test specimens.

This data also includes a comparison of the bend strength between as-welded specimens with the upper and lower halves of the bimetallic joint face subjected to compressive or tensile loading. Two tests of the Bend B with its coupon top surface facing upward, which puts the lower half of the bimetallic joint face in tensile loading, resulted in an average maximum bending force of 10.34 kN. The inverted Bend B specimens that had the upper half of the bimetallic joint face in tensile loading exhibited maximum bend loads nearly half of the opposing orientation. The remaining heat-treated bend specimens and shear test specimens were then heat-treated with the aging only process.

Table 7 – Bend Test Results of Heat-Treatment Study

	Bend Strength (kN)		
Heat Treatment	Bend A	Bend B (top up)	Bend B (top down)
T6511	0.21	2.63	- - -
aging only	2.63	11.37	- - -
as-welded	2.72	10.34	5.92

b) ***Bending*** – Bending tests for several bimetallic joint orientations and heat-treatment conditions were conducted according to *ASTM E-290: Standard Test Methods for Bend Testing of Material for Ductility* procedures. Results are shown in Table 8.

Table 8 – Bend Test Results of Best Parameter Specimens

	Mean Bend Strength (kN)		
Heat Treatment	Bend A	Bend B (top up)	Bend B (top down)
aging only	2.72	11.28	5.11
as-welded	2.72	10.34	5.92

c) ***Shear*** – *ASTM D1002: Standard Test Method for Apparent Shear Strength of Single-Lap-Joint Adhesively Bonded Metal Specimens by Tension Loading (Metal-to-Metal)* procedures were used to determine the shear strength at the bimetallic interface. Results are shown in Table 9.

Table 9 – Shear Test Results of Best Parameter Specimens

Heat Treatment	Qty. of Specimens	Mean Shear Strength (MPa)
aging only		
as-welded		

As of May 31, 2013, the final shear test specimens are being machined. Final shear test strength results will be provided upon completion of shear testing in mid June.

d) ***Tensile*** – As discussed above, the tensile test data representing the best FSP parameter set were from tensile tests conducted during the parameter optimization experiments discussed in Section D.3.a. These tests resulted in a mean coupon tensile strength of 205 MPa. Figure 20 compiles the tensile strength vs. strain graphs for each of the five test specimens.

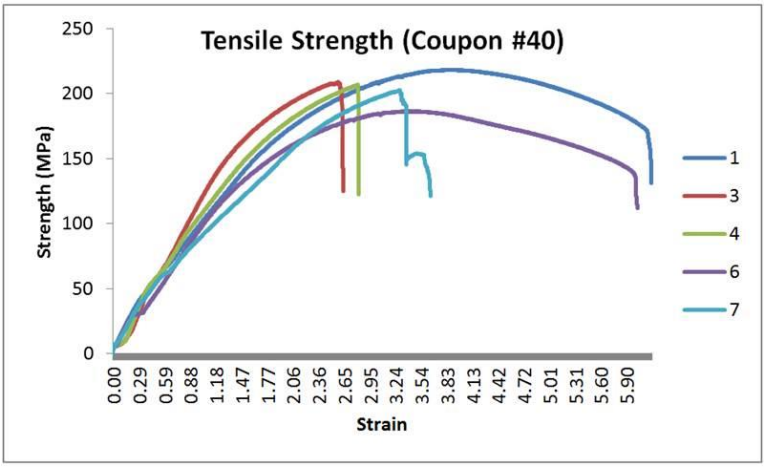

Figure 20 – Tensile Strength vs. Strain of Best Parameter Specimens

F. FRICTION STIR WORK PIECE PRE-HEATING SYSTEM

One work directive task of this project was to design, build, and demonstrate a FSP work piece pre-heating system for the purpose of reducing FSP tool wear when processing hard materials, e.g. armor steel and titanium alloys. Several such auxiliary heating methods have been used in conjunction with frictional heating including induction, oxyacetylene flame, and laser methods. Induction was chosen as the method to implement for this project because of the availability of a suitable induction power source system at Focus: HOPE.

1. Induction Heating Principles– The basic operating theory of heating materials by electrical induction can be illustrated with a simple electrical circuit as shown in Figure 21. This circuit includes a source of AC current which passes thru an electrical coil. The second part of the simplified circuit is a grounded resistor and is not physically connected to the AC coil section and no current passes from one to the other. However the AC current passing through the coil does induce an equal and opposite secondary current, much like the primary and secondary coils of an electrical transformer, which then creates heat as it flows through the electrical resistor. In reality, the second section of this example circuit is not an electrical resistor but is a metal work piece that has resistive properties. The electromagnetic force, or flux, created when the work piece is placed near the AC coil does induce current flow in the work piece which is often called eddy currents. The changing magnetic field caused by the alternating source current creates swirls, or eddies, of local electrical fields which flow thru the conductive metal that is bounded within the physical space of the current's space. Since the work piece metal has electrical resistivity, it is heated as the current passes thru it (Figure 22).

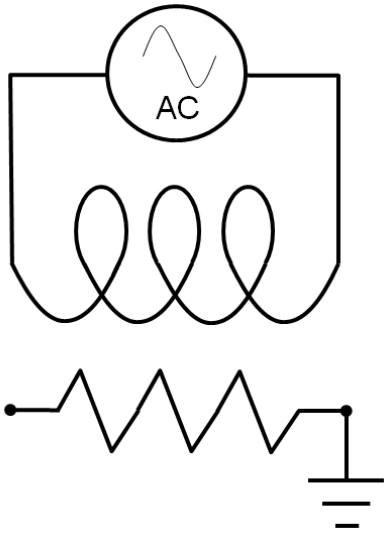

Figure 21 – Schematic of Induction

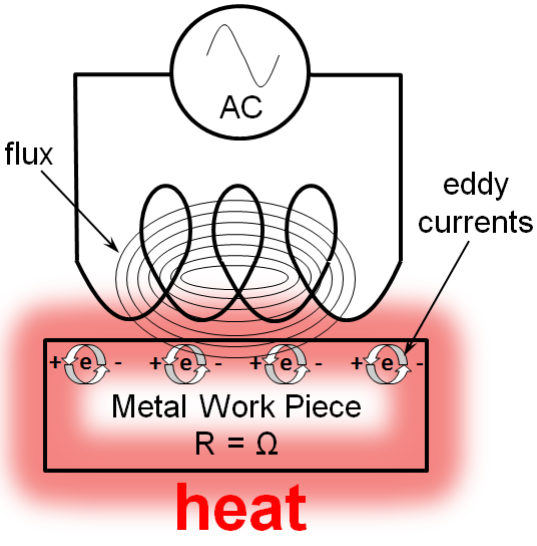

Figure 22 – Heat Created by Induced

2. System Design Description – The overall induction pre-heating system that was designed and assembled for this project is comprised of six sub-systems as shown in Figure 23.

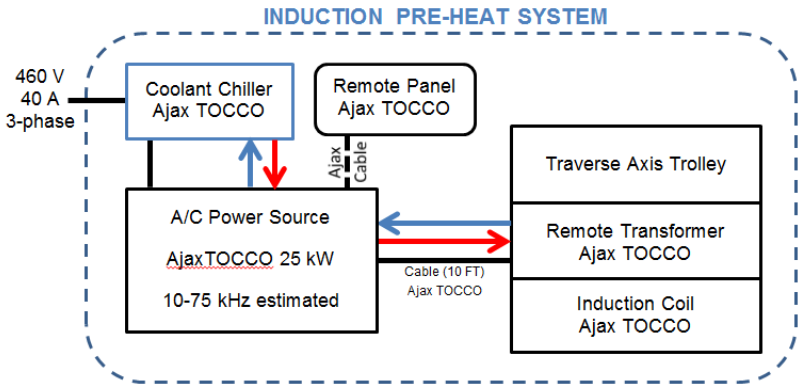

Figure 23 – Schematic of Induction Pre-Heating System

a) ***A/C Power Source*** – Ajax TOCCOtron 25 kW (Figure 24-a)
b) ***Fluid Cooling System*** – Koolant Coolers Model (Figure 24-b)
c) ***Power Source Control Panel*** – Ajax/TOCCO Remote Panel (Figure 24-c)
d) ***Remote Transformer & Cable*** – Ajax/TOCCO 350 KVA HHT (Figure 24-d)
e) ***Induction Coil*** – custom by Ajax/TOCCO (Figure 24-e)
f) ***Trolley/Carriage Assembly*** – custom extruded aluminum frame components (Figure 24-f)

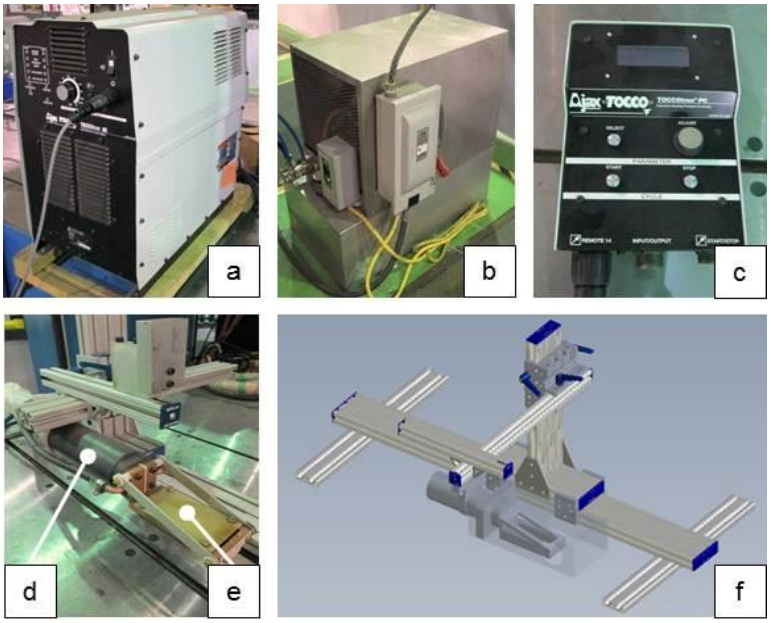

Figure 24 – Induction Pre-Heating Sub-Systems

The A/C power source, cooling system, and control panel that were used for this project had previously been used as part of a heat-treating system that was

integrated into a FH CNC machining center. After consultation with local Ajax/TOCCO personnel, this equipment was confirmed as adequate for this pre-heating application and the equipment was removed from the machining center. An induction coil that was part of that heat-treating system was available but unsuitable for application to this project's material and fixture configuration. A new coil subassembly that was designed specifically for this application (1/2-in. thick steel and 1 ½-in. wide heat zone) was purchased along with an application-specific remote transformer to which the coil would be mounted. The remote transformer assembly also included a 10-ft. long power cable which connected to the A/C power source and cooling system supply and return lines for the water-cooled coil.
Several alternatives for mounting the induction coil and controlling its motion as an auxiliary system to the FSP spindle and tool were considered. These options included: mounting the coil assembly to a linearly self-propelled carriage that would travel along the surface of the work pieces ahead of the traversing FSP tool and suspending the coil assembly from the FSP machine's spindle frame so that the coil was physically coupled with the FSP tool positioner. Ultimately for simplicity and portability, a sliding trolley/carriage mounted to an extruded aluminum linear bearing frame was chosen as the method to mount the coil assembly and control its position relative to the in-process FSP tool. See Appendix C for a design layout of the trolley assembly. With this arrangement, the coil trolley would be pushed ahead of the tool by the spindle frame. Figure 25 is a photo showing the coil/remote transformer assembly in position during a friction stir process. An arrow indicates the point of contact location between the spindle frame and the trolley carriage.
The trolley assembly has a single degree of freedom (along the traverse Y-axis) but features several mechanisms that allow adjustment of the X (side-to-side) and Z (vertical) axes positions of the coil assembly, relative coil-to-tool spacing, and overall trolley frame location with respect to the work piece fixture.

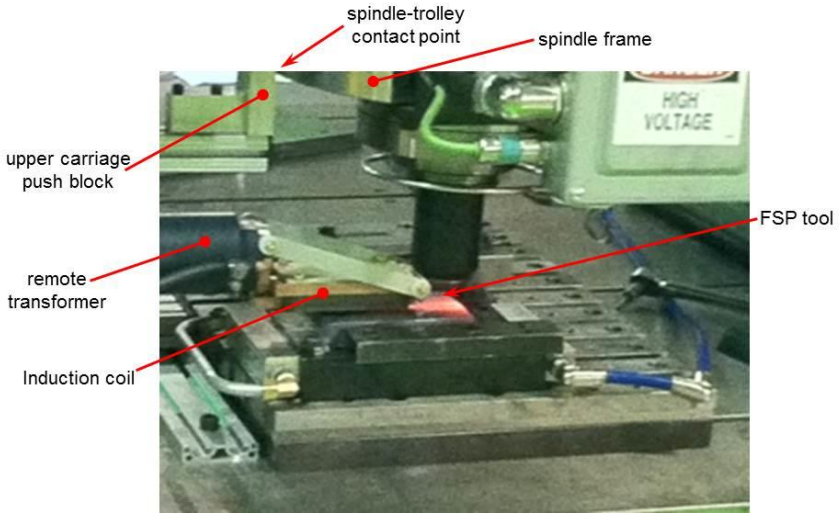

Figure 25 – Induction Coil in Operation

3. Evaluation Results – During an initial trials period, we evaluated several induction process parameter variations and developed a procedure and spindle motion program to heat the plunge area of the work pieces immediately before and during the friction stir process. The Ajax/TOCCO power source and controller include a series of process parameter selection screens that provide for a programmable heating cycle profile (See Figure 26). The pre-heating cycle would begin with the induction coil positioned over the plunge point of the FSP cycle with approximately 1/8-in. gap between the work piece surface and the bottom face of the coil. The FSP spindle was positioned at a probe height approximately 1-mm above the work piece surface with a traverse axis gap of approximately ½-in. between the spindle frame and the coil trolley push block. Level 1 of the heat cycle would warm the work piece to 400-600°C. The heat cycle would advance to Slope 1, the FSP spindle would move to the plunge point while pushing the coil trolley to a position above the traverse path, and the FSP tool would plunge into the work pieces. As the heat cycle advanced to Level 2, the FSP traverse motion would begin. After approximately 33% of the traverse had been completed, the heat cycle would begin Slope 2 which decreased the induction heat input to offset the increasing friction stir process heat. After approximately 67% of the traverse had been completed the heat cycle would reach Level 3. Because of the distance between the FSP tool and the edge of the induction heat zone (60-80 mm), the effective heat zone of the coil was eventually pushed beyond the work pieces where it would have minimal heating effect on the friction stir process. Therefore the heat cycle would end when the coil reached this position, but the FSP traverse would continue to its end. Table 10 lists the profile program parameters and several examples of pre-heating cycles that were evaluated.

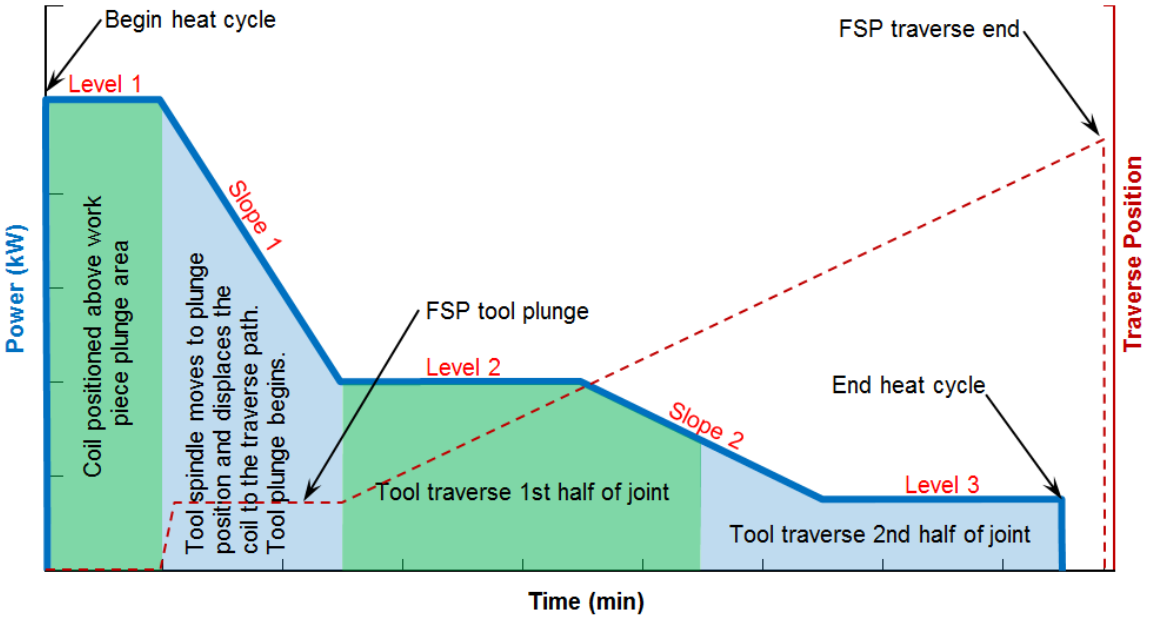

Figure 26 – Induction Pre-Heating Cycle

Table 10 – Induction Heating Cycle Parameters

	Level 1		Slope 1 (min)	Level 2		Slope 2 (min)	Level 3	
	Power (kW)	Time (min)		Power (kW)	Time (min)		Power (kW)	Time (min)
A	10.0	1.0	1.5	4.0	2.0	2.0	1.5	2.0
B	12.0	1.0	0.5	6.0	1.5	2.0	2.0	1.5
C	18.0	0.5	0.5	0.0	0.0	0.0	0.0	0.0

The major obstacle that we experienced in implementing this pre-heating method was aluminum melting; either during the pre-heating process or during the friction stir process when the FSP tool was self-generating heat. The fundamental reason for this issue is the large difference in material melting temperatures (582 °C for AA6061 vs. 1300-1400 °C for steel) combined with intentionally adding heat for the purpose of elevating the steel's temperature toward its solidus temperature. After many process and equipment revisions, the two solutions which prevented melting of the aluminum alloy were the addition of a cooled clamp bar to the aluminum side of the work piece fixture (see Figure 4) and offsetting the centerline of the coil trolley path and the joint centerline so that the induction heat zone was confined to the steel work piece only (see Figure 27).

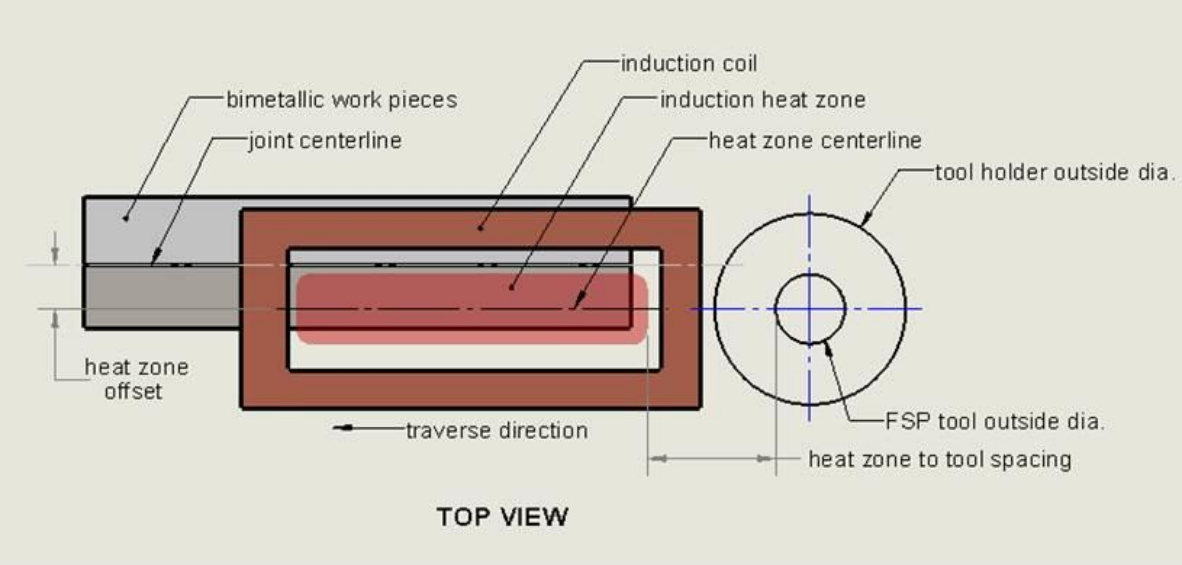

Figure 27 – Induction Heat Zone Offset

Nine bimetallic FSP coupons were fabricated using various heat zone offset positions and a common FSP parameter set (300 rpm, 25 mm/min, 1.0 mm offset, and 3° back tilt). While the coupons did not exhibit excessive aluminum melting, many did have surface discontinuities and exposed wormholes along the joint face area. To minimize heat transfer into the aluminum yet provide sufficient auxiliary heating for the steel, the heat zone was positioned so that the steel-side clamp block (made of tool steel) was receiving the direct induction heat which then conducted the heat into the steel work piece. In essence, the heat zone offset was greater than the width of the steel work piece plus ½ of the width of the heat zone. This admittedly unorthodox induction heating arrangement resulted in joint coupons without surface or sub-surface discontinuities.

Table 11 lists the tensile test results and corresponding induction heat cycle parameters for the two acceptable joint coupons. Because these strength tests results were significantly lower than previous results without pre-heating and also because of the heat transfer issues relating to the melting points of the dissimilar metals, we decided that auxiliary heating was not effective for this bimetallic application and ceased development and evaluations.

Table 11 – Induction Pre-Heating Tensile Strength Results

Coupon	Level 1		Slope 1 (min)	Level 2		Slope 2 (min)	Level 3		Specimen Quantity	Mean Tensile (MPa)
	Power (kW)	Time (min)		Power (kW)	Time (min)		Power (kW)	Time (min)		
44	12.0	0.5	0.1	0.0	0.0	0.0	0.0	0.0	5	132.6
45	15.0	0.5	0.1	0.0	0.0	0.0	0.0	0.0	5	123.0

With common FSP parameters - 300 rpm, 25 mm/min, 1.0 mm offset, and 3° back tilt)

4. Recommendations (Pre-Heating System) – The induction pre-heating system described above was ill-suited for the disparate melting temperatures of the dissimilar alloys of this study, aluminum and steel. Heating the steel work piece in an effort to reach its plastic state would allow for a larger bimetallic joint offset because of lower loading of the FSP tool which theoretically would promote metallurgical mixing of the alloys and thus a stronger joint. As evidenced by FSP tool breakage and wear when the bimetallic joint offset was increased beyond 1-mm and the limited bimetallic mixing exhibited, the hardness and resulting lack of mechanical deformation of the high hardness steel armor was an obstacle to improved dissimilar joint integrity. Promoting steel plasticity during a bimetallic friction stir process is essential for a robust bimetallic weld joint. Therefore we make the following recommendations for further investigation, evaluation, and development of auxiliary pre-heating during bimetallic FSP:

   a) ***Heat Extraction from Aluminum Work Piece*** – While the addition of a cooled clamp bar to the aluminum side of the fixture reduced or eliminated the aluminum melting issue, further development of aluminum heat management techniques is required. Computer modeling of the heat transfer which occurs during a bimetallic FSP (with and without auxiliary heating) will be very helpful for this analysis.

   b) ***Induction Heat Zone Location*** – The rectangular shape and design of the induction coil and the FSP tool holding system prevented the proper location of the induction heat zone with respect to the in-process FSP tool. With the trailing edge of the induction coil heat zone being located ahead of the FSP tool center along the traverse axis, the minimum heat zone-to-FSP tool spacing possible with this project's configuration was approximately 42-mm (see Figure 27). For this arrangement to be effective, the programmed heat cycle would need to provide heat levels that would adequately warm the work pieces to a plastic state temperature but with a time delay between the application of heat energy and actual material deformation by the FSP tool. Also the thermal gradients within the work pieces caused by varying amounts of frictional heat input (plunge, dwell, or traverse) and different conduction/convection heat transfer properties resulting from fixture design variations (e.g. clamp points, fastener holes, exposed surfaces). In essence finding the right induction heat cycle program was like shooting at a moving target.

      For future investigations of inductive pre-heating, we recommend two improvements to counter this issue of heat cycle time lag. First, having an induction coil concentrically located around the FSP tool with shielding that would decouple the electromagnetic forces on the trailing side of the tool would provide proper heat application to the work piece directly ahead of the traversing FSP tool. Besides revising the coil design accordingly, the FSP tool holding system that has been developed throughout this contract will also need to be revised to allow the coil to abut the rotating tool. Second the development and use of a heat transfer model to include the bimetallic work pieces and their fixture, FSP tool system, and auxiliary

heating and thermal management systems to predict the in-process work piece temperatures would assist with reducing or controlling heat losses and improving process consistency.

In conclusion, despite its development and use during this bimetallic FSP investigation, auxiliary pre-heating by any supplementary energy source would be better suited for the FSP of harder, higher temperature materials. Because of relatively small joint offsets investigated for this aluminum/steel application (compared to all-aluminum FSP), aggressive tool wear was avoided and the true objective of this auxiliary heating system, to reduce FSP tool wear, was not properly evaluated. However, had the system been more developed and effective at bringing the steel work piece to a plastic state without adversely affecting the aluminum work piece, higher bimetallic joint offsets would have been investigated and the FSP tool would have been subjected to the factors affecting tool wear.

G. OVERALL SUMMARY

1. Project Findings and Conclusions

a) Within the FSP process parameters envelop that was studied during this project two general trends linking bimetallic joint strength to a particular process parameter were apparent: tensile strength increased as traverse speed was increased, and tensile strength decreased as tool rotation speed was increased.
b) The tensile failure of the better performing bimetallic joint coupon test specimens occurred away from the bimetallic joint face with the ductile fracture aligned with the thermo-mechanically affected zone (TMAZ) of the aluminum side of the joint. This indicates that the overall strength capability of this bimetallic joint is dependent on the post-FSP metallurgy of the aluminum alloy and may be further improved with appropriate heat treatment methods.
c) FSP tools fabricated from tungsten-rhenium (W-Re) alloy that included a small percentage of hafnium-carbide (HfC) often failed prematurely with the fracture appearing to emanate from material voids of dislodged HfC particles. Without improved manufacturing methods for the W-Re-HfC material, this particular alloy may not be suitable for the friction stir process applied to hard, high strength materials.
d) The relatively high mechanical bending loads placed onto the FSP tool during a bimetallic joining process with at least one of the alloys having high strength and hardness must be considered when designing the tool. When applied to other relatively softer materials, the main emphasis of FSP tool design (other than plastic deformation material flow) is usually limited to durability and wear resistance caused by the rotational motion of the tool. However when applied to high strength alloys, the structural integrity of the FSP tool and its resistance to non-rotational loads is of equal design importance.
e) The FSP tools used during this project that were fabricated from lanthanated tungsten (W-La) alloy had very low wear resistance which indicates that this particular alloy may not be suitable for the friction stir environment.
f) Micro-hardness analyses of the bimetallic joint shows that the hardness of the steel was lowered as a result of the friction stir process by 45% at the bimetallic joint interface but retained its original hardness in areas away from the joint face. The aluminum material hardness was the lowest (35% less than base material) in the TMAZ of the FSP joint, which is typical for heat-treatable aluminum alloys. The failure point of tensile test specimens commonly occurred at this TMAZ location of the bimetallic joint.
g) Microscopic analysis shows that in the areas where the steel hardness was lowered the most the martensitic microstructure was tempered most likely because of the affected material experienced slow cooling after the localized frictional heat of the process had been traversed away from the cooling material.
h) Microstructure analysis of the aluminum joint material using Electron Back Scatter Diffraction (EBSD) revealed that the material that had been directly stirred by the FSP tool had undergone dynamic recrystallization induced by severe plastic deformation at relatively high temperature which resulted in the material's grain size being reduced to 5-10 µm from the 100-500 µm original grain size of for the base material.
i) Energy Dispersive Spectroscopy (EDS) to determine the elemental distribution of the material at the bimetallic interface showed that a 1-2 µm thick aluminum-iron diffusion

zone links the two separate dissimilar alloys to form a metallurgical bond. The thickness of this intermetallic material increased slightly near the top of the bimetallic joint face probably due to the higher local temperatures generated by the frictional heat source at the top surface. Failure analysis of some tensile test specimens indicated that failures that occurred at the joint interface, as opposed to the TMAZ of the aluminum material, were brittle fractures of the upper portion of the joint interface material. This brittle nature is typical of intermetallic material between dissimilar alloys.

j) Bend tests indicate that the upper portion of the bimetallic joint interface is roughly half as strong as the lower portion which corresponds to the thicker layer of brittle intermetallic material occurring along the upper joint interface.

k) The final strength of the bimetallic FSP joint material is directly affected by aluminum alloy heat treatment processes. The joint strength was significantly degraded by submitting the entire joint to the T6511 heat treatment of the original AA6061 base material. However bimetallic material subjected to only precipitate hardening (aging) and not solution hardening of the T6511 procedures, exhibited marginally higher strength.

l) Effective thermal management of process heat by using heat sinks, external work piece and fixture cooling, and auxiliary heating systems is required when using FSP to join dissimilar metals that have significantly different melting temperatures. For this project, the application of a water-cooled heat sink in direct contact with the aluminum work piece seemed to improve joint strength by 10-12%.

m) Auxiliary heating methods for the purpose of softening the higher temperature alloy of a bimetallic joint must be closely coupled with the machine control system and its resulting FSP process parameters to be effective. However with the significant difference in melting temperatures of the aluminum and steel of this project, the use of auxiliary heating for this particular bimetallic joint is difficult.

2. Technical Feasibility of Bimetallic Friction Stir Process

This project successfully demonstrated that joining the dissimilar metals of AA6061 and HHA steel is feasible using a standard 5-axes friction stir machine, tungsten-rhenium alloy FSP tool with a tapered probe design, and external heat extraction from the aluminum side of the joint coupon. Bimetallic joint coupons exhibited tensile strengths that exceeded that of a similar AA6061-to-AA6061 friction stir joint with tensile test failures occurring at the thermo-mechanically affected zone of the aluminum alloy side of the FSP joint. Table 12 compares relevant material and joint strengths.

Although several of the tungsten-rhenium alloy FSP tools suffered failure and excessive erosion wear, the better performing tools showed minimal wear after 15 separate FSP events that had yielded approximately 100 total lineal inches of metallurgically-bonded bimetallic material joint.

Table 12 – Tensile Strength Comparison

MATERIAL / WELD TYPE	Yield Strength (MPa)
AA6061-T6511	
base material	345 [a]
arc/fusion welded	124 [b]
FSW	194 [c]
High Hardness Steel (HHS)	
base material	1034 [d]
arc/fusion welded	tbd
AA6061/HHS FSW joint	205 [e]

[a] Kaiser Aluminum Certified Test Report, Lot #Z00222015

[b] AWS Welding Handbook, Vol. 3, Material and Applications, p. 13

[c] at FHI April 2011

[d] ATI Allegheny Ludlum 500-MIL™

3. Recommendations for Future Development

a) ***Extended length bimetallic joints*** – To assist the Army with its goal of reducing the weight of ground vehicles, development of this aluminum-steel joint should continue with the objective of attaining the capability to fabricate continuous 36-in. long bimetallic joints. This effort would also require the design and fabrication of a fixture to hold extended length work pieces and incorporate appropriate thermal management features.

b) ***Tool life and cost*** - Improving FSP tool life and/or reducing tool cost would support the development of extended length joints. To extend tool life the use of auxiliary heating for the steel side of the bimetallic joint should be further investigated. Along with the recommendations of Section F.4 above, resistance and ultrasonic methods are other possible heat sources that could be applied as a means to warm the steel alloy to a proper FSP working temperature with minimal effect on the aluminum temperature.

Currently the only tool materials capable of withstanding the high temperatures, loading, and wear-inducing friction of the friction stir environment and have successfully demonstrated their applicability are tungsten-based alloys and synthetic cubic boron nitride. Molybdenum alloy and boron carbide have also been evaluated. Because of the base elements involved, these alloys are expensive. Based on our experience with the current FSP tool system, a revised second generation design for the FSP tool and tool holding system would reduce the amount of tool alloy required and minimize material costs.

c) ***Continue joint development*** – In addition to the factors involved with developing the process and hardware for extended length bimetallic joints, many other aspects that may improve joint strength should be studied. The addition of a separate alloying material between the aluminum and steel alloys would affect the intermetallic compounds formed at the joint as a result of the friction stir process. Alternative tool probe and joint face configurations, along with joint designs, would increase the bimetallic surface area and introduce mechanical interlocking features. The use of machine force control, opposed to the positional control used throughout this project, would also affect joint strength.

d) ***Investigate other alloys*** – AA6061 was selected for this project solely because of its availability in our material stock at the time. However other aluminum alloys are more applicable for the construction of ground vehicles; 2000, 5000, and 7000 series. Similar or expanded studies of bimetallic FSP joints using these materials, as well as other steel alloys, should be conducted

APPENDIX A – Coupon Specimen Tensile Test Results

Coupon[1]	Tensile Yield Strength (MPa) Coupon Specimen #								Coupon Mean (MPa)
	1	2	3	4	5	6	7	8	
20	137.3	151.4	130.85						139.9
21A	35.36	57.24	79.33						57.3
21B	78.8	51.79							65.3
22A	134.93	123.36	158.06						138.8
22B	128.89								128.9
23	171.74	150	116.5						146.1
24A	154.4	152.25	121.81	137.85	125.62				138.4
25A	152.24	165.72	156.86	152.51					156.8
25B	137.35	133.49	127.84	133.93					133.2
26B	102.86	126.68	165.5	132.54	141.78				133.9
28A	182.08	175.61	178.42						178.7
28B	190.8	164.01	173.26						176.0
30	135.42	136.26							135.8
32	98.84	103.18	129.42	115.12	112.96	112.47			112.0
34A	169.65	166.75	164.62	205.08	167.45				174.7
34B	199.24	175.38	168.32	198.77					185.4
35	162.42	203.31	147.74	116.34	151.51				156.3
36	117.65	120.97	135.71	134.97	134.77	138.28			130.4
37A	111.73	115.47	176.55	146.22	173.68	133.56			142.9
37B	164.21	186.31	171.77	150.42	163.53	180.44			169.4
39A	163.9	144.14	172.86	134.42	167.76	137.19			153.4
39B	156.22	166.52	177.85	160.29	162.76				164.7
40	218.16	208.65	206.78	186.34	202.48				204.5
53[2]	186.87	190.3	160.93	160.97	212.63				182.3
54A	146.41	134.53	141.73						140.9
54B	120.02	133.97	133.88	125.74	148.42				132.4
55	154.57	150.05	142.55	139.59	174.55				152.3
56	184.74	186.35	195	195.28	222.85	192.47	201.42	173.86	194.0
57	169.96	181.08	180.38	185.94	185.41				180.6
58	104.23	173.06	179.19	152.57	141.94				150.2
59	x x x	155.71	114.5						135.1
60[3]	x x x	146.87	176.87						161.9
61	168.04	179.49	147.92	149.41	184.46				165.9
62	121.08	159.52	173.17	162.52	182.61				159.8
63	166.28	133.08	164.49	129.79					148.4
64	174.83	115.23	147.65	108.7					136.6
65	x x x	155.09	154.56						154.8
66		173.61	181.26	189.04	186.74				182.7
76[4]	132.89	135.58	152.72						140.4
77	x x x	129.78	116.72	123.67	149.34				129.9
78	131.44	162.97	131.42	147.27	159.48				146.5

[1] *Coupons with visual defects were not tested.*
[2] *Without aluminum side cooled clamp bar.*
[3] *For Runs 60 and later, a positional offset to correct the A and B rotational axes angles was used.*
[4] *Cooling system corrections (tube routing, tank filled)*

APPENDIX B – Test Specimen Extraction and Machining Drawings

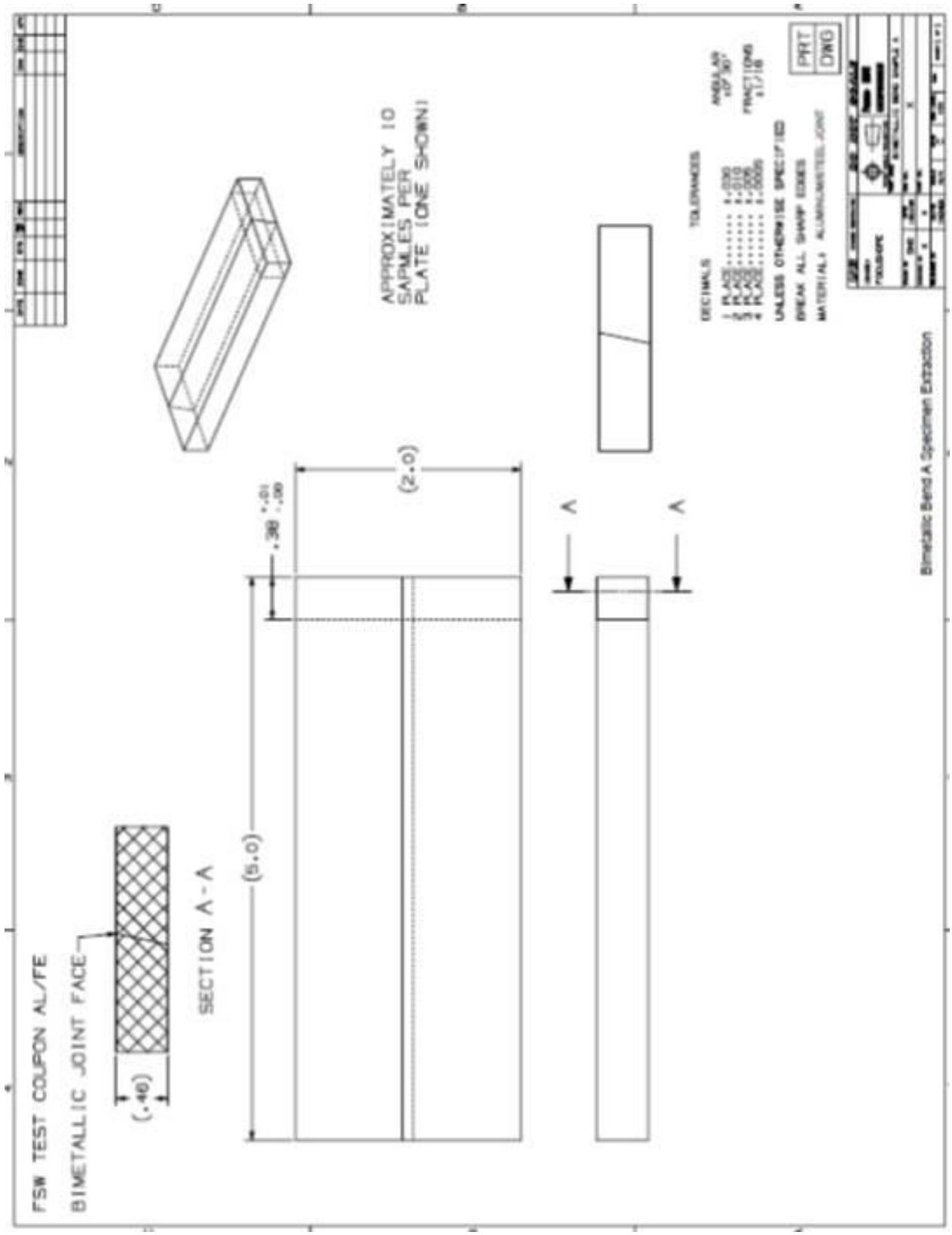

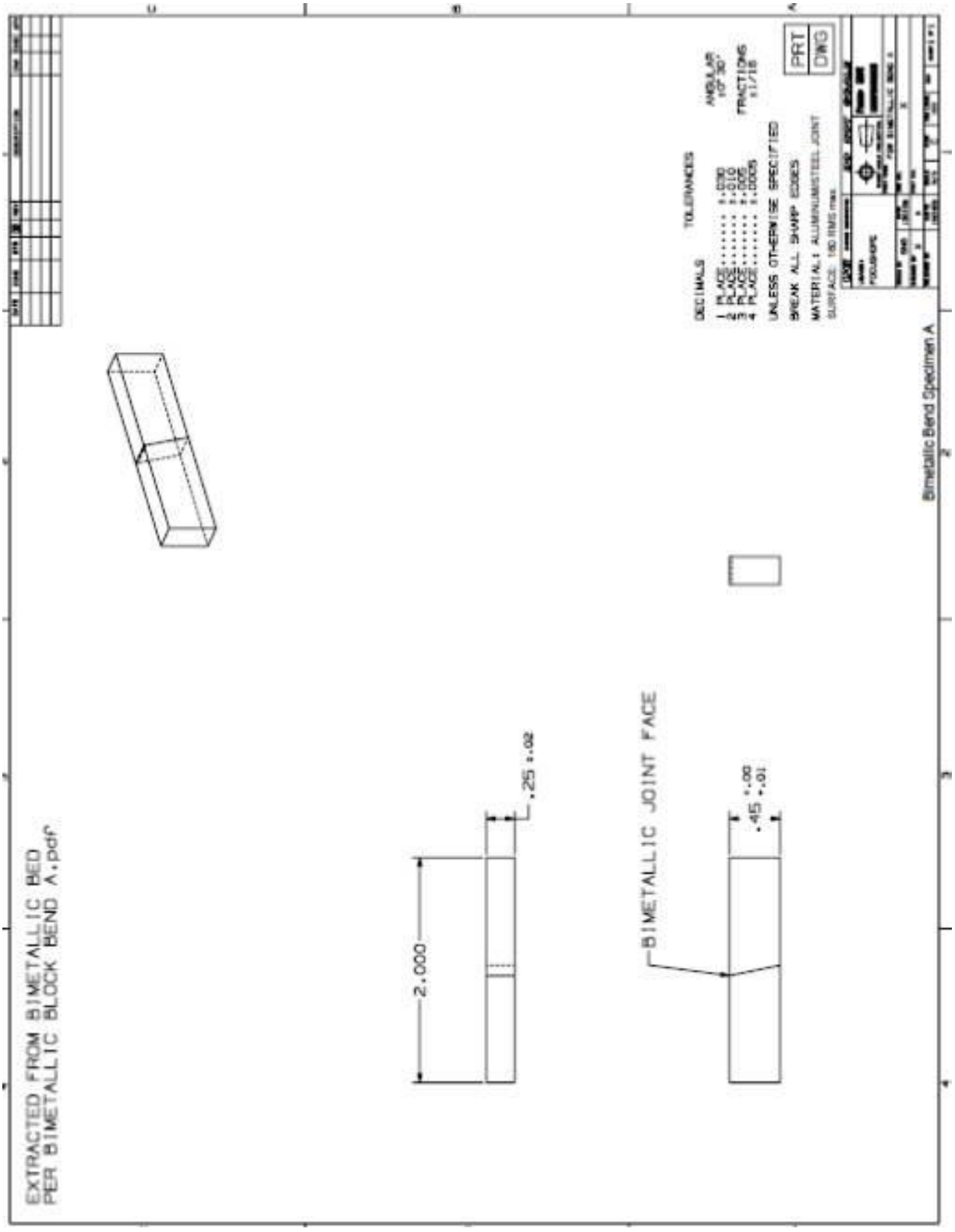
EXTRACTED FROM BIMETALLIC BED
PER BIMETALLIC BLOCK BEND A.pdf
Bimetallic Bend Specimen A
BIMETALLIC JOINT FACE
2.000
.25 ±.02
.45 +.00 -.01
UNLESS OTHERWISE SPECIFIED
BREAK ALL SHARP EDGES
PART
DWG

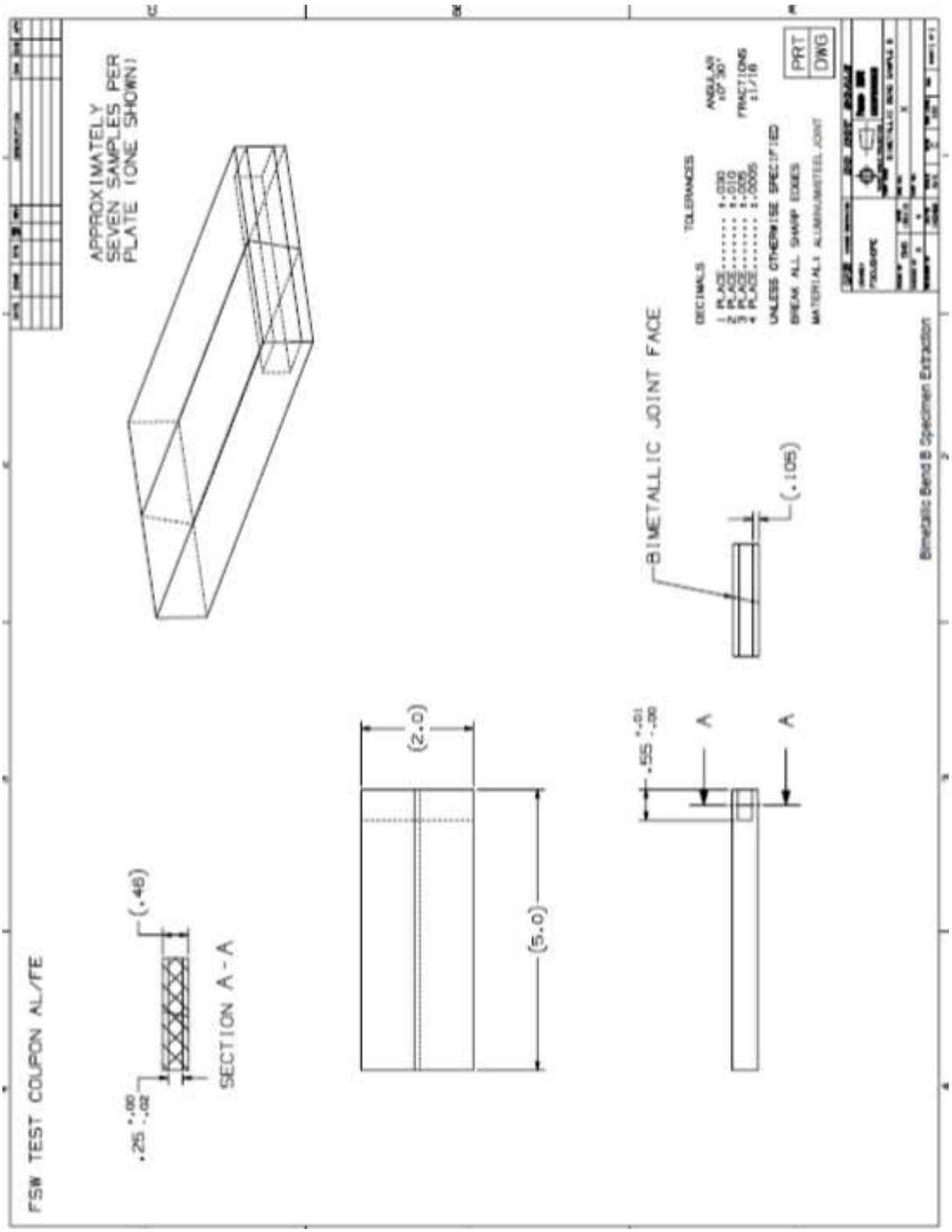
APPROXIMATELY SEVEN SAMPLES PER PLATE (ONE SHOWN)
BIMETALLIC JOINT FACE
(.105)
(2.0)
(5.0)
.55 +.01 -.06
A
A
(.46)
.25 +.00 -.02
SECTION A-A
FSW TEST COUPON AL/FE
Bimetallic Bend & Specimen Extraction
PRT
DWG

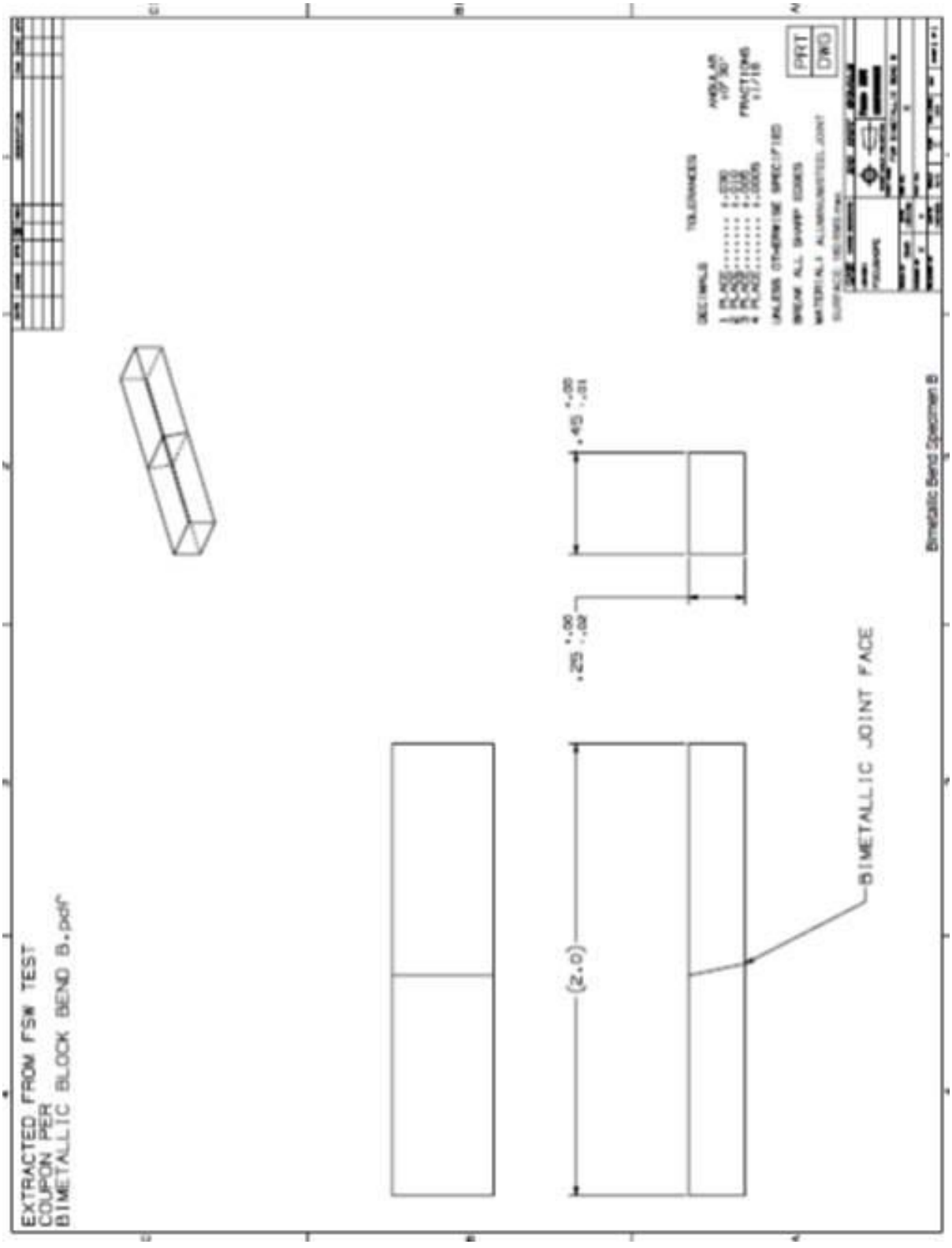
EXTRACTED FROM FSW TEST
COUPON PER
BIMETALLIC BLOCK BEND B.pdf
BIMETALLIC JOINT FACE
(2.0)
.45 +.05 -.01
.25 +.05 -.03
Bimetallic Bend Specimen B
PART
DWG

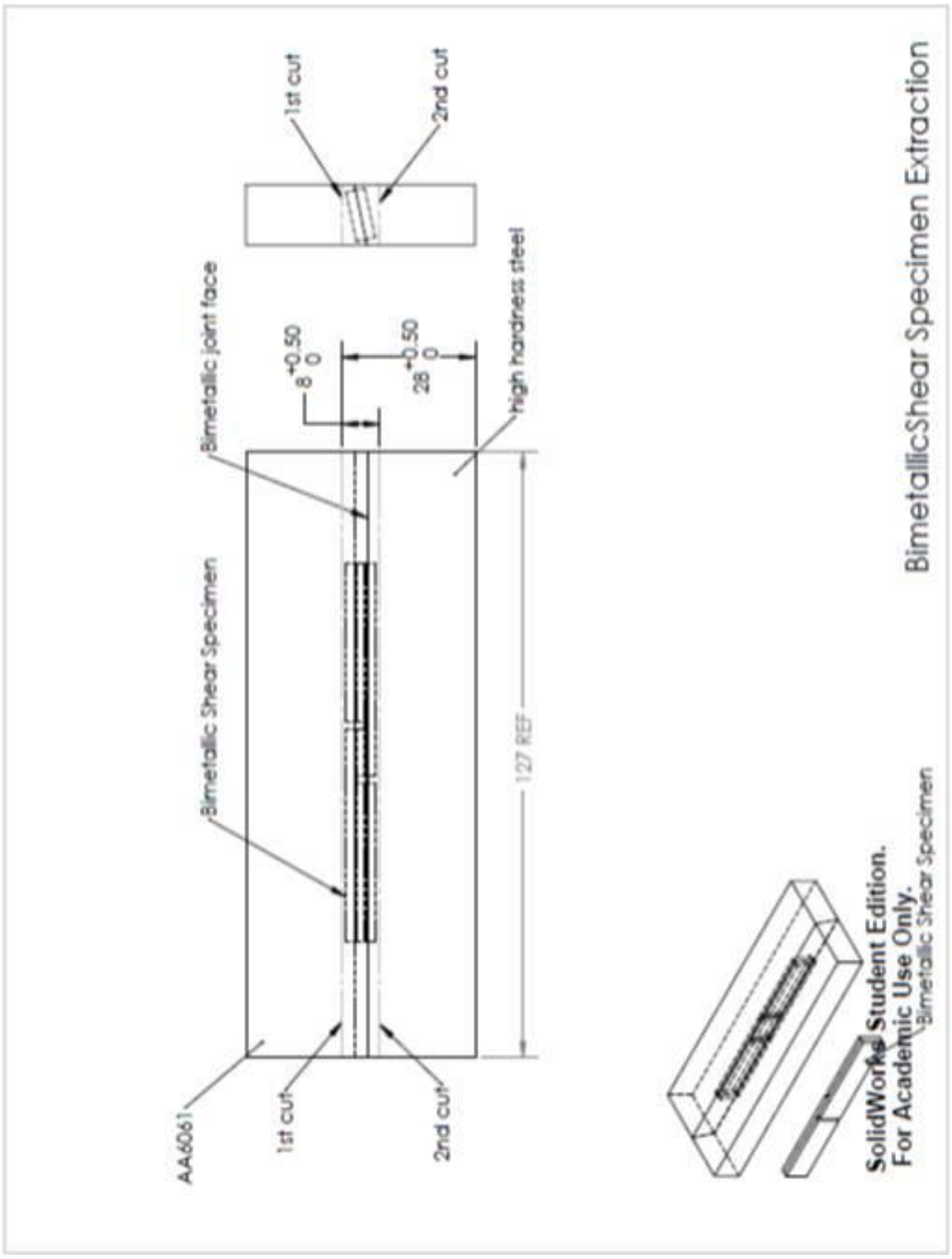
BimetallicShear Specimen Extraction
1st cut
2nd cut
Bimetallic joint face
high hardness steel
Bimetallic Shear Specimen
127 REF
AA6061
1st cut
2nd cut
SolidWorks Student Edition.
For Academic Use Only.
Bimetallic Shear Specimen

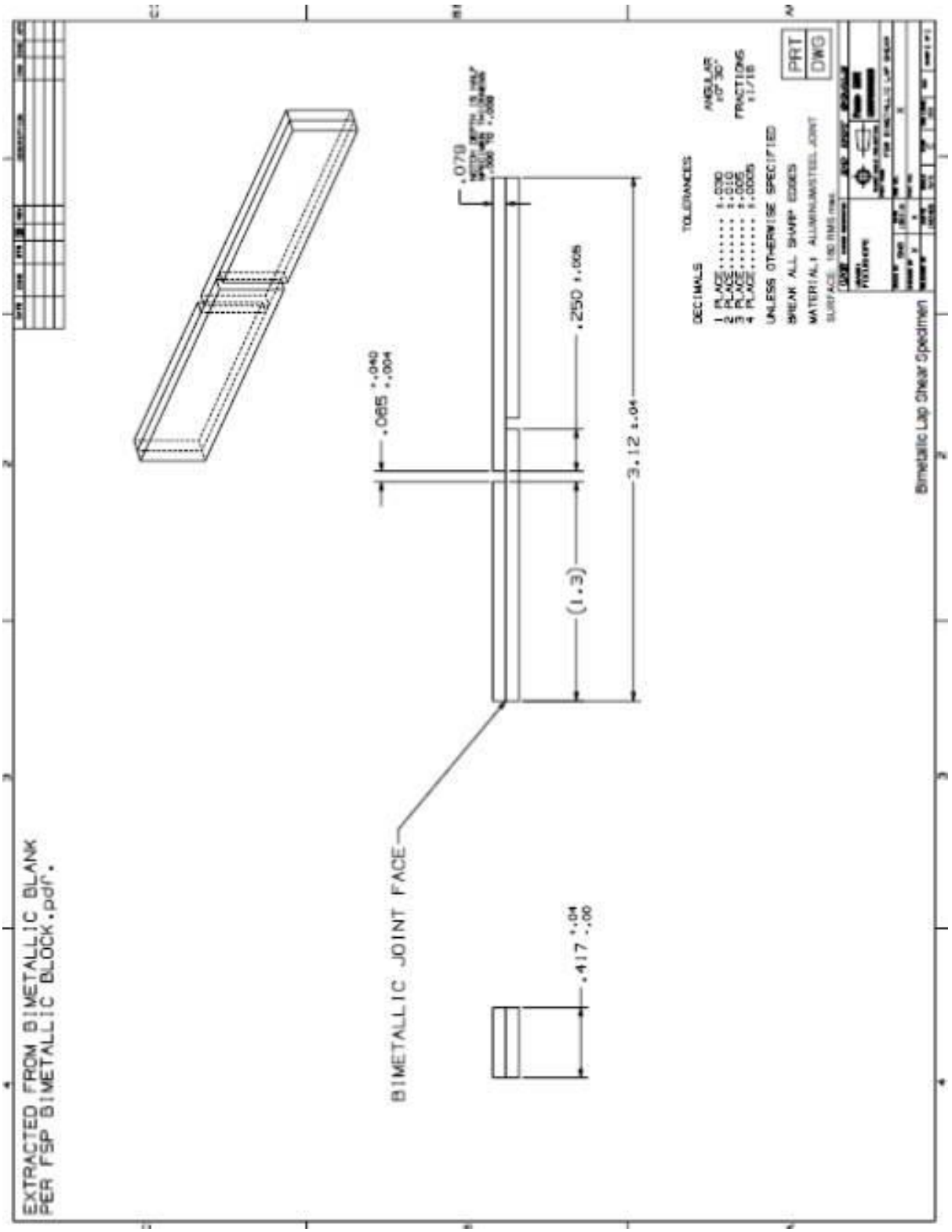
EXTRACTED FROM BIMETALLIC BLANK
PER FSP BIMETALLIC BLOCK.pdf*.
BIMETALLIC JOINT FACE
.078
.085 +.040 +.004
.250 ±.005
3.12 ±.04
(1.3)
.417 +.04 +.00
TOLERANCES
DECIMALS
1 PLACE ±.030
2 PLACE ±.010
3 PLACE ±.005
4 PLACE ±.0005
ANGULAR ±0° 30'
FRACTIONS ±1/16
UNLESS OTHERWISE SPECIFIED
BREAK ALL SHARP EDGES
MATERIAL ALUMINUM/STEEL JOINT
PRT
DWG
Bimetallic Lap Shear Specimen

APPENDIX C – Pre-Heating Coil Trolley Assembly